HYDRONAUTICS, Incorporated

TECHNICAL REPORT 703-2

SUPERCAVITATING CASCADES WITH CONSTANT PRESSURE CAMBERED BLADES

By

B. Yim

July 1967

Prepared Under

National Aeronautics and Space Administration
George C. Marshall Space Flight Center
Contract No. NAS 8-20625

TABLE OF CONTENTS

LIST OF FIGURES

NOTATION

a_o, a_1, a_3	Points in the ζ plane corresponding to the end of foil, and the end points of upper and lower cavity respectively
A,B,C,D	Defined in Equation [20]
c	Chord length of foil
C_L	Lift coefficient defined by Equation [4]
C_D	Drag coefficient defined by Equation [27]
d	Distance between leading edges of adjacent two foils in the cascade
$F = F_r + iF_i$	Function defined in Equation [12-0]
k	Strength of a singularity at the leading edge
k_1	Curvature at the leading edge
ℓ	Cavity length
P_1, P_2, Q_1, Q_2	Defined in Equation [19]
$P_{-\infty}, P_c$	Pressure at $x = -\infty$ and on the cavity respectively
p	Perturbation pressure
$q_2 = \lvert u_2 + iv_2 \rvert$	Total speed at $x = \infty$
u,v	x,y components of perturbation velocity respectively
U	Speed at $x = -\infty$

w	Complex velocity potential
$z = x + yi$	Coordinate in the physical plane
γ	Stagger angle defined in Figure 1
σ	Cavitation number defined in Equation [1]
ρ	Density of water
$\zeta = \xi + \eta i$	Coordinates in the transformed plane

INTRODUCTION

For the design of many types of high speed axial flow machines such as pumps and compressors operating under stalled or heavily cavitating conditions, perhaps the most well defined and simple model corresponds to the flow through supercavitating cascades. Betz and Petersohn (1931) solved the exact two dimensional problem for the flow through flat plate cascades with infinite cavities using the free streamline theory of Kirchhoff and Helmholtz. Then Cohen and Sutherland (1958) solved the linearized version of the supercavitating flat plate cascade problem with finite cavities using the theory developed by Tulin (1953). Later Acosta (1960) applied the same linearized free streamline theory to the choked flow past a cascade of circular arc hydrofoils. Stripling and Acosta (1962) made an exact nonlinear calculation for partial cavitation in a cascade of flat plates of semi-infinite chord. Wade (1963) solved the linearized problem for partial cavitation in cascades of flat plate hydrofoils.

For an isolated single supercavitating hydrofoil, it has been well understood that the camber of the foil very much influences the characteristics of the hydrofoil such as its lift coefficient and lift-drag ratio, since Tulin and Burkart (1955) developed the linearized two dimensional theory of optimum hydrofoils by a transformation into the aerofoil plane. Auslaender (1962) calculated the shapes of such foils together with their cavity shapes and found that the cavity had negative thicknesses

unless an extra leading edge singularity was superposed. Auslaender also considered a foil shape with a constant pressure distribution; in this case the cavity thickness is not negative; and this shape is quite similar to a Tulin two-term optimum camber with a slight angle of attack. (Tulin and Burkart, 1955). Thus, the constant pressure camber seems to be quite attractive in the design of hydrofoils as well as of aerofoils. (See Abbott and Doenhoff, 1959).

In addition, nonlinear theory for the supercavitating constant pressure cambered foils is not too difficult to solve, as in the case of flat plate foils. In general, the free nonlinear streamline theory for the given curved boundary is quite complicated to solve with an integral equation to solve (Sedov 1965, Jacobsen 1964). The second order theory for the constant pressure camber is also quite simple if we use the same scheme adopted by Tulin (1963), since the second order problem has exactly the same form as the first order problem.

The present report is concerned with a linearized theory on the flow through a supercavitating cascade with a constant pressure camber. For the cavity, Tulin's double spiral model (1963) is used; this model was proved to do very well in predicting physical quantities (Yim, 1964). Each flow through a foil in a cascade is transformed into a half plane by the same conformal mapping used by Acosta (1960). A simple boundary value problem is solved in the transformed plane with the boundary conditions given on a straight line and at the point which corresponds to

negative infinity in the physical plane. The numerical computations were performed on an IBM 1130 at HYDRONAUTICS, Incorporated. The relations between drag coefficients, cavitation numbers and lift coefficients are plotted for many solidities and stagger angles. The foil shapes and the cavity shapes are also plotted.

FORMULATION OF THE BOUNDARY VALUE PROBLEM

We consider a cascade with the stagger angle γ and solidity c/d where c is the chord length of a foil and d is the distance between the leading edges of adjacent foils as shown in Figure 1a. The flow at infinity far in front is uniform with the velocity $\overline{U}$. The flow through each foil can be considered to be periodically repeated. We consider a complex coordinate $z = x + yi$ with the origin at the leading edge of a foil and the x axis parallel to $\overline{U}$, as shown in Figure 1a. When the angle of attack and the thickness of the foil are small, then the perturbation due to the cascade can be considered to be small. Thus the linearization of the perturbation velocity can be allowed for the first approximation, and the boundary condition can be applied at the x axis.

When we neglect viscosity, we can consider the perturbation complex velocity $w(z) = u - iv$ which is analytic except at singularities. We consider a cavity starting from the leading edge of the foil and ending behind the foil. The pressure inside the cavity is the vapor pressure and the speed at the free streamline is constant. If we use the cavitation number

$$\sigma = \frac{P_{-\infty} - P_c}{\frac{\rho}{2} U^2} \qquad [1]$$

where $P_{-\infty}$ is the pressure at $x = -\infty$, and P_c is the pressure in the cavity, the Bernoulli equation gives us within the linear approximation

$$\frac{u}{U} = \frac{\sigma}{2} \qquad [2]$$

on the cavity, and everywhere in the flow

$$\frac{2u}{U} = - \frac{p}{\frac{1}{2}\rho U^2} = \frac{P_{-\infty} - P}{\frac{1}{2}\rho U^2} \qquad [3]$$

where p is the perturbation pressure. Now, if we assume that the pressure on the foil is constant, then u/U is also a constant, say λ, then the lift coefficient of the supercavitating foil will be

$$C_L = \frac{L}{\frac{1}{2}\rho U^2 c} \doteq \frac{P - P_c}{\frac{1}{2}\rho U^2} = \sigma - 2\lambda \qquad [4]$$

where L is the lift force. This will be useful later for the representation of our solution in terms of C_L rather than λ.

Tulin's double spiral model assumes the pressure behind the cavity is constant equal to the pressure at $x = \infty$ all the way on the wake boundary. The pressure at $x = \infty$ and the length of cavity can be obtained by the condition at $x = -\infty$ and the wake closure condition. Thus, in effect, u is given everywhere on $y = \pm 0$, $x > 0$ with the condition at ∞. Namely, if we use u,v,p as nondimensional quantities for u/U, v/U, $p/(\frac{1}{2}\rho U^2)$ respectively,

$$\left.\begin{array}{llll} u = \sigma/2 & \text{on} & y = +0 & 0 < x < \ell \\ u = \sigma/2 & \text{on} & y = -0 & 1 < x < \ell \\ u = \lambda & \text{on} & y = -0 & 0 < x < 1 \\ u = u_2 & \text{on} & y = \pm 0 & \ell < x < \infty \\ u = 0 & \text{at} & x = -\infty & \end{array}\right\} \qquad [5]$$

as is shown in Figure 1b. The distance ℓ represents cavity length. The wake closure condition can be written in the linear approximation as

$$\int_{\infty}^{0} v(x,-0)\, dx + \int_{0}^{\infty} v(x,+0)\, dx = 0 \qquad [6]$$

It will be shown that this condition is actually equal to the condition of continuity between the upstream and the downstream of the cascade. In order that the analytic function w(z) has a

unique solution with the above boundary conditions, it is also required that the conditions at all the juncture points should be specified (see e.g. Muskhelishvili 1953) such as the kind of singularities or zeros at the points $0, -a_0, a_1, -a_3$, as shown in Figure 16.

CONFORMAL MAPPING

We consider the mapping

$$z = e^{i\gamma} \log\left\{1 - \zeta\, e^{i\left(\frac{\pi}{2} - \gamma\right)}\right\} + e^{-i\gamma} \log\left\{1 - \zeta\, e^{-i\left(\frac{\pi}{2} - \gamma\right)}\right\} \quad [7]$$

where $\zeta = \xi + i\eta = e^{i\left(\frac{\pi}{2} - \gamma\right)}$ corresponds to

$$z = -\infty\, e^{-i\gamma} + (2m\pi + \delta)\, e^{i\left(\frac{\pi}{2} - \gamma\right)}$$

$$0 \leq \delta < 2\pi$$

and is considered to be the branch point; and the cut by a straight line from this point to $\zeta = \infty\, e^{i(\pi/2 - \gamma)}$ makes z single valued in the upper half of the ζ plane. $|\zeta| = \infty$ is mapped to $x = \infty$. By one crossing of this cut line, z will be increased by $2\pi\, e^{i(\pi/2 - \gamma)}$; thus $\zeta = 0$ corresponds to $z = 2m\pi\, e^{i(\pi/2 - \gamma)}$ with $m = 0, \pm 1, \pm 2, \ldots\ldots$ which are the leading edges of all the foils with $d = 2\pi$. Therefore any flow passing a foil of the cascade can be mapped by the flow in the upper half of the ζ plane. It

suffices to consider the flow passing a single member of foils, say the case of m = 0. Then, when ζ is real, z is also real. By a little algebra we can easily see

$$x = \cos\gamma \log\{1 - 2\xi \sin\gamma + \xi^2\} - 2\sin\gamma \arg(1 - \xi\sin\gamma - i\xi\cos\gamma) \qquad [8]$$

where $-\pi < \arg < \pi$. By a differentiation with respect to ξ we obtain

$$\frac{dx}{d\xi} = \frac{2\xi\cos\gamma}{1 - 2\xi\sin\gamma + \xi^2} \qquad [9]$$

Since the scale of length is already set by $d = 2\pi$, the corresponding point $-a_o$ for the chord length c cannot be set arbitrarily but depends on the solidity c/d. The cavity length ℓ depends mainly on the cavitation number σ in our problem. However we may give ℓ instead of σ and find σ which corresponds to ℓ. Thus if we give a point $\xi = -a_o$ and $\xi = a_1$ in the transformed plane for the chord length and the cavity length, respectively, this will decide $x = c$, and $x = \ell$ from [8] giving the solidity and the cavity length. The corresponding point $\xi = -a_3$ for $y = -0$, $x = \ell$ can be obtained by solving for a_3 in

$$\ell = \cos\gamma \log\left(1 + 2a_3 \sin\gamma + a_3^2\right) - 2\sin\gamma \tan^{-1}\frac{a_3\cos\gamma}{1 + a_3\sin\gamma} \qquad [10]$$

numerically by Newton-Raphson's method or others.

Now our problem is to solve for $w(z(\zeta)) = u(\xi,\eta) - iv(\xi,\eta)$ which is an analytic function of ζ except at singularities, with the boundary conditions on $\eta = 0$ as follows

$$\left.\begin{array}{lll} u = \frac{\sigma}{2} & \text{on} & 0 < \xi < a_1 \quad \text{and} \\ & & -a_3 < \xi < -a_o \\ u = \lambda & \text{on} & -a_o < \xi < 0 \\ u = u_3 & \text{on} & -\infty < \xi < -a_3 \quad \text{and} \\ & & a_1 < \xi < \infty \end{array}\right\} \qquad [11]$$

We consider a singularity at $\zeta = 0$ behaving like $k/(\pi i\zeta)$ which is tantamount to having a single vortex in the transformed plane at $\zeta = 0$ with the strength kU/π. This has often been considered for additional cavity thickness (see Johnson and Starley 1962 or Auslaender 1962) or a point drag cavity model (e.g. Yim 1962). Otherwise we do not consider any extra singularity because at juncture points for the end of the cavity the desirable singularity is logarithmic, and at the trailing edge if there was no

zero, the logarithmic singularity there may be at most tolerable as in the case of an aerofoil camber of constant pressure (Abbott and Doenhoff, 1959).

SOLUTION

To obtain the solution, it is rather convenient to solve for

$$F(\zeta) \equiv F_r(\xi,\eta) + iF_i(\xi,\eta) = w(\zeta) - u_\infty + iv_\infty \qquad [12\text{-}0]$$

where $-v_\infty$ is the imaginary part of the complex velocity at $x = \infty$ (or $|\xi| = \infty$). Then our boundary condition will change for $F(\zeta)$:

$$\left.\begin{aligned} F_r &= \frac{\sigma}{2} - u_\infty \quad \text{on} \quad 0 < \xi < a_1 \quad \text{and} \\ & \qquad\qquad -a_3 < \xi - a_o \\ F_r &= \lambda - u_\infty \quad \text{on} \quad a_o < \xi < 0 \\ F_r &= 0 \quad \text{on} \quad -\infty < \xi < -a_3 \quad \text{and} \\ & \qquad\qquad a_1 < \xi < \infty \end{aligned}\right\} \qquad [12]$$

The solution for this is given by

$$F(\zeta) = \frac{1}{\pi i}\int_{-\infty}^{\infty} \frac{F_r(t)}{t - \zeta} \qquad [13]$$

By substitution of [12] and performing integration we obtain

$$F(\zeta) = \frac{1}{\pi i}\left\{\left(\frac{\sigma}{2} - u_3\right) \log \frac{(a_o + \zeta)(\zeta - a_1)}{(a_3 + \zeta)\zeta} + (\lambda - u_3) \log \frac{\zeta}{a_o + \zeta} + \frac{k}{\zeta}\right\} \qquad [14]$$

Since

$$w(\zeta) = 0 \quad \text{at} \quad \zeta = e^{i\left(\frac{\pi}{2} - \gamma\right)}$$

$$\text{or at } z = -\infty \qquad [15]$$

$$F(\zeta) = -u_3 + iv_3 \quad \text{at} \quad \zeta = e^{i\left(\frac{\pi}{2} - \gamma\right)} \qquad [16]$$

Now we consider the wake closure condition [6] in the physical plane and notice w(z) is periodic having exactly the same value at the corresponding points with respect to each foil of the cascade. We also notice w(z) in the flow has no singularity except at the boundary. Thus Equation [6] can be rewritten referring to Figure 1a

$$\mathrm{Im} \int_{B_\infty A_1 A_0 O A_3 B_\infty} w(z)\, dz = \mathrm{Im} \int_{B_\infty A_3 O D_\infty D_\infty' O' A_3' B_\infty' B_\infty} w(z)\, dz = 0$$

Since $w(z) = 0$ at $z = -\infty$ in addition,

$$\mathrm{Im} \int_{B_\infty' B_\infty} w(z)\, dz = \mathrm{Im} \int_{B_\infty' B_\infty} (u_2 - iv_2)\, d\,(y \tan \gamma + iy) = 0$$

This should be true for any length of d or $B_\infty' B_\infty$. Hence

$$u_2 = v_2 \tan \gamma \qquad [17]$$

This relation can also be obtained by the continuity relation of flow. Namely

$$U \cos \gamma = q_2 \cos (\alpha_2 + \gamma)$$

$$= (U + u_2) \cos \gamma - v_2 \sin \gamma$$

where q_2 is the total speed at $z = \infty$ and

$$q_2 \cos \alpha_2 = U + u_2 \quad , \quad q_2 \sin \alpha_2 = v_2$$

Hence

$$u_2 = v_2 \tan \gamma$$

Now if we substitute the boundary condition at $z = -\infty$ expressed by [16] into our solution [14], and separate the imaginary and the real part, we will obtain two simultaneous equations for σ and u_2, with a little algebra as follows,

$$\left.\begin{aligned} \frac{\sigma}{2} Q_1 + u_2 Q_2 &= -\lambda \log \left|\frac{C}{D}\right| - k \sin \gamma \\ \frac{\sigma}{2} P_1 + u_2 P_2 &= -\lambda \arg \frac{C}{D} + k \cos \gamma \end{aligned}\right\} \qquad [18]$$

where

$$\left.\begin{aligned} Q_1 &= \log \left|\frac{A}{B}\right| \\ Q_2 &= -\log \left|\frac{A}{B}\right| - \log \left|\frac{C}{D}\right| + \pi \cot \gamma \\ P_1 &= \arg \frac{A}{B} \\ P_2 &= -\arg \frac{A}{B} - \arg \frac{C}{D} + \pi \\ 0 &< \arg < 2\pi \end{aligned}\right\} \qquad [19]$$

with

$$\left.\begin{aligned} A &= a_o \sin\gamma - \cos 2\gamma - a_o a_1 - a_1 \sin\gamma \\ &\quad + i(a_o \cos\gamma + \sin 2\gamma - a_1 \cos\gamma) \\ B &= a_3 \sin\gamma - \cos 2\gamma + i(a_3 \cos\gamma + \sin 2\gamma) \\ C &= \sin\gamma + i\cos\gamma \\ D &= a_o + \sin\gamma + i\cos\gamma \end{aligned}\right\} \quad [20]$$

Thus using [4] we obtain from [18]

$$\frac{\sigma}{C_L} = \frac{R_1}{1 + R_1} - \frac{k}{C_L}\frac{R_3}{1 + R_1} \quad [21]$$

$$\frac{u_2}{C_L} = \left(\frac{1}{2} - \frac{R_1}{2(1 + R_1)}\right) R_2 + \frac{k}{C_L} R_4 \quad [22]$$

where

$$\left.\begin{aligned} D_1 &= Q_1 P_2 - Q_2 P_1 \\ R_1 &= \left(P_2 \log\left|\frac{C}{D}\right| - Q_2 \arg\frac{C}{D}\right) \Big/ D_1 \\ R_2 &= \left(Q_1 \arg\frac{C}{D} - P_1 \log\left|\frac{C}{D}\right|\right) \Big/ D_1 \\ R_3 &= (P_2 \sin\gamma + Q_2 \cos\gamma)/D_1 \\ R_4 &= (Q_1 \cos\gamma + P_1 \sin\gamma)/D_1 \end{aligned}\right\} \quad [23]$$

FOIL SHAPE AND DRAG COEFFICIENT

From the linearized streamline equation

$$\frac{dy}{dx} = \frac{v}{1+u} \approx v \qquad [24]$$

we can obtain the shapes of foils and cavity just by integrating [24]

$$y = f(x) = \int_0^x v(x,0)\, dx$$

$$= \int_0^{x(\xi)} v(x(\xi),0)\, \frac{dx}{d\xi}\, d\xi \qquad [25]$$

or

$$\frac{y}{cC_L} = \frac{f(x)}{c\,C_L} = \frac{2\cos\gamma}{\pi c} \int_0^{x(\xi)} \left\{ \left(\frac{\sigma}{2C_L} - \frac{u_2}{C_L} \right) \log \left| \frac{(\xi - a_1)(a_o + \xi)}{(a_3 + \xi)\xi} \right| \right.$$

$$+ \left(\frac{1}{2} - \frac{\sigma}{2C_L} - \frac{u_2}{C_L} \right) \log \left| \frac{\xi}{a_o + \xi} \right| + c\pi \frac{u_2}{C_L} \cot\gamma$$

$$\left. + \frac{k}{C_L \xi} \right\} \frac{\xi\, d\xi}{1 - 2\xi\sin\gamma + \xi^2} \qquad [26]$$

The drag coefficient is

$$C_D = \frac{D}{\frac{1}{2}\rho U^2 c} \doteq -\frac{1}{c}\int_0^c (\sigma - 2\lambda)\,\frac{dy}{dx}\,dx + \frac{2k^2}{\pi c}$$

$$= -\frac{C_L}{c}\int_0^{-a_o} v(x(\xi),0)\,\frac{dx}{d\xi}\,d\xi + \frac{2k^2}{\pi c} \qquad [27]$$

The last term in [27] is a pure cavity drag which is obtained by application of Blasius' theorem

$$d(X - iY) = \tfrac{1}{2} i\rho w^2\, dz \qquad [28]$$

where the left hand side represents the force at dz.

When we integrate around a small circle around the origin

$$\tfrac{1}{2}\, i\rho \oint w^2(z)\, dz = \tfrac{1}{2}\, i\rho \oint w^2(\zeta)\,\frac{dz}{d\zeta}\,d\zeta$$

$$= \tfrac{1}{2}\,\rho \oint \frac{k^2\, 2i}{\pi^2\,\zeta}\,d\zeta$$

$$= \rho\,\frac{k^2}{\pi} \qquad [29]$$

If we compare [17], [25] and [26] we can immediately see that

$$\frac{C_D}{C_L^2} = -\frac{f(c)}{cC_L} + \frac{2k^2}{\pi c C_L^2} \qquad [30]$$

The integral [26] is integrated numerically with due care about the intervals in the ζ plane since the correspondence between ξ and x behaves quite differently when $|\xi| < 10$ from the case of $|\xi| > 10$ as shown in Figure 2.

CASE OF INFINITE CAVITY LENGTH

In this case, our solution corresponding to [14] in $0 \leq z \leq c$ is

$$F(\zeta) = \frac{1}{\pi i}\left[\left(\frac{\sigma}{2} - u_2\right)\left\{\log \frac{-(a_o+\zeta)}{\zeta} - \pi \tan\gamma\right\} + (\lambda - u_2)\log\frac{\zeta}{a_o+\zeta} + \frac{k}{\zeta}\right] \qquad [31]$$

since from [8]

$$\lim_{a_1 \to \infty}\left(\frac{a_1}{a_3}\right) = e^{-\pi \tan\gamma} \qquad [32a]$$

and in Equation [20]

$$A = (-a_o - \sin\gamma - i\cos\gamma)e^{-\pi\tan\gamma}$$
$$B = \sin\gamma + i\cos\gamma \qquad [32b]$$

Otherwise, nothing changes in all the equations for the case of finite cavities. However, it may be worth noting here that this result may be a little different from that obtained by the condition at $x = \infty$, $u = \sigma/2$ since here $u = u_\infty < 0$ at $x = \infty$ although $u = \sigma/2 > 0$ at the cavity whose length is infinitely long, yet closes at infinity.

CASE OF ZERO SOLIDITY

This is the case of an isolated supercavitating foil with constant pressure camber and with the double spiral cavity model. For this, the conformal mapping corresponding to [7] is

$$z = \zeta^2 \qquad [33]$$

This may be obtained from the limit ($d \to \infty$) of

$$z = \frac{d}{2\pi}\left[e^{i\gamma} \log\left\{ 1 - \frac{\zeta}{\sqrt{\frac{d}{2\pi}\cos\gamma}}\, e^{i\left(\frac{\pi}{2} - \gamma\right)} \right\} + e^{-i\gamma} \log\left\{ 1 - \frac{\zeta}{\sqrt{\frac{d}{2\pi}\cos\gamma}}\, e^{-i\left(\frac{\pi}{2} - \gamma\right)} \right\} \right] \qquad [34]$$

which is essentially equivalent to [7], by a Taylor's series expansion of log. In this case, $u_\infty = 0$. Hence, from [14]

$$w(\zeta) = \frac{1}{\pi i}\left\{\frac{\sigma}{2}\log\frac{(a_o+\zeta)(\zeta-a_1)}{(a_3+\zeta)\zeta} + \lambda\log\frac{\zeta}{a_o+\zeta} + \frac{k}{\zeta}\right\} \qquad [35]$$

For the application of the wake closure condition [6] in this case, we expand [35] for large ζ

$$w(\zeta) = \frac{1}{\pi i}\left[\frac{1}{\zeta}\left\{a_o\left(\frac{\sigma}{2}-\lambda\right) - \sigma a_1 + k\right\} + \cdots\cdots\right] \qquad [36]$$

To have

$$\mathrm{Im}\oint w(z)dz = 0$$

$$(y = \pm 0, \quad x > 0)$$

we should have

$$\mathrm{Im}\oint w(z)dz = 0$$

$$|z| \to \infty \qquad [37]$$

since there is no singularity in the flow. Thus the coefficient of $\frac{1}{\zeta}$ in [36] must be zero. Namely

$$a_o\left(\frac{\sigma}{2}-\lambda\right) - \sigma a_1 + k = 0 \qquad [38]$$

From [4], [33] and [38] we obtain

$$\frac{\ell}{c} = \frac{a_1^2}{a_o^2} = \frac{1}{\sigma^2}\left(\frac{C_L^2}{4} + \frac{k^2}{c} + \frac{kC_L}{\sqrt{c}}\right) \qquad [39]$$

which gives the cavity length.

The foil shape and the drag coefficient are obtained by using

$$\frac{dx}{d\xi} = 2\xi \qquad [40]$$

in [25] and [27] instead of [9]. In this case, the integration can be performed in a closed form and we have

$$\frac{y}{cC_L} = \frac{f(x)}{cC_L} = \frac{2}{\pi}\left[\frac{\sigma}{2C_L}\left\{\frac{x_1 - \ell_1}{2}\log\left|\frac{\sqrt{x_1} - \sqrt{\ell_1}}{\sqrt{x_1} + \sqrt{\ell_1}}\right| - \sqrt{\ell_1 x_1}\right\} + \frac{1}{2}\left\{\frac{x_1 - 1}{2}\log\left(\sqrt{x_1} + 1\right) - x_1 \log x_1 + \frac{\sqrt{x_1}}{2}\right\} + \frac{k\sqrt{x_1}}{C_L\sqrt{c}}\right] \qquad [41]$$

where

$$x_1 = x/c \quad \text{and} \quad \ell_1 = \ell/c > 1 \qquad [42]$$

$$\frac{C_D}{C_L^2} = \frac{2}{\pi}\left[\frac{\sigma}{2C_L}\left\{\frac{\ell_1 - 1}{2}\log\frac{1+\sqrt{\ell_1}}{1-\sqrt{\ell_1}} + \sqrt{\ell_1}\right\} + \frac{1}{4} + \frac{k}{C_L\sqrt{c}} + \frac{k^2}{C_L^2 c}\right] \quad [43]$$

CURVATURE AT LEADING EDGES

The strength of the singularity at the leading edge k is related to the curvature of the leading edge of the foil. When we consider cavity shapes near the leading edge in Equation [26], the curvature k_1 at the leading edge will be represented approximately by the value at $(y = +0,\ x = +0)$ of

$$k_1 = \frac{d^2y/dx^2}{\{1 + (dy/dx)^2\}^{\frac{3}{2}}} \quad [44]$$

From [24]

$$\left.\begin{aligned}\frac{dy}{dx} &= \frac{v(\xi(x))}{1+\sigma/2}\\ \frac{d^2y}{dx^2} &= \frac{1}{1+\sigma/2}\frac{dv(\xi)}{d\xi}\frac{d\xi}{dx}\end{aligned}\right\} \quad [45]$$

From [7], [9] and [34] we may write

$$\frac{dx}{d\xi} = \frac{\xi}{1 - \frac{2\xi \sin\gamma}{\sqrt{\frac{d}{2\pi}\cos\gamma}} + \frac{2\pi\xi^2}{d\cos\gamma}} \qquad [46]$$

From [14], [44], [45] and [46] we obtain by taking the limit of $\xi \to 0$

$$k_1(\xi \to 0) = \frac{\pi^2}{k^2}\left(1 + \frac{\sigma}{2}\right)^2$$

or the radius of curvature at the origin can be represented by

$$\frac{\rho_1}{c} = \frac{1}{k_1 c} = \frac{k^2}{\pi^2 c\left(1 + \frac{\sigma}{2}\right)^2}$$

DISCUSSION OF NUMERICAL RESULTS

The relation between the drag coefficient C_D, the cavitation number σ, and the lift coefficient C_L are shown in Figures 3-8 for different stagger angles γ and different solidities c/d, by curves of C_D/C_L^2 versus σ/C_L for $k = 0$. Thus if we have γ and c/d, then any two values of C_D, σ, and C_L will decide the rest of them. As is clear in Equation [30], C_D/C_L^2 is the same as $y/(C_L c)$ at $x/c = 1$ for $k = 0$. Therefore this may be interpreted as equal to $-\alpha/C_L$ where α is the angle of attack within our

approximation. The limiting cases are also shown in Figures 3-8 for the infinite cavity length in the cascades and for the case of zero solidity which is the case of an isolated cavitated foil solved by Auslaender (1962) for zero cavitation number. It has already been known (Auslaender 1962) that the constant pressure camber isolated foil has four times as large lift coefficient as that due to a flat plate foil for the same angle of attack. However, when the solidity increases, the lift coefficient of the constant pressure camber decreases for the same angle of attack as shown in Figure 21. This will be discussed more later.

The length of cavity has a sensitive relation with the drag-lift ratio. The shorter is the former, the less is the latter. However since it is known from experiments (Wade and Acosta 1967) that the cavity is unstable in either the case of an isolated foil or of cascades when the cavity length chord ratio is near 1 (< 1.25) the designer may well avoid this area. In Figures 9-12 the lengths of cavities are also shown. It appears that, for each cavity chord ratio, there is an optimum stagger angle where C_D/C_L^2 is minimum.

The shapes of cambers are shown in Figures 16-21 in terms of $y/(C_L c)$ versus x/c. Naturally a flat plate parallel to the stream is the limiting shape of $C_L = 0$ for any solidity or stagger angles. For the case of $k = 0$ (or when the radius of curvature at the leading edge is zero) camber shapes correspond to shock free entry, i.e. the flow is tangent to the foil at the leading edge. It seems that the camber is not too sensitive to

either the length of the cavity or the cavitation number, for the pressure to be uniform on the foil. Mainly the change of angle of attack seems to be able to adjust the uniformity of pressure. However, the camber is decreasing when the solidity becomes larger for the same angle of attack. This seems to be the reason why the lift coefficient of the constant pressure camber becomes as small as in the case of flat plates for large solidities, as shown in Figure 21.

According to our formulation of the problem, the stagger angle is not the same as the conventional one which is smaller by the angle of attack α which is not known a priori than our nominal stagger angle γ. The actual stagger angle can be interpolated easily in Figures 9-12. The conventional inlet angle of the flow is equal to γ. The flow exit angle β_2 can be calculated from the values of u_2 which is given in Figures 13-14 by

$$\beta_2 = \gamma - \tan^{-1} \frac{u_2 \cot \gamma}{1 + u_2}$$

The influence of the curvature at the leading edge on the drag coefficient is shown in Figure 15 from equation in the case of an isolated foil of constant pressure camber.

Examples for foil shapes are given in Figures 16-19. Examples for cavity and foil shapes with zero leading edge radii are shown in Figure 20.

The numerical results of finite cavity problems, especially of such as cavity lengths, heavily depend upon the model assumed at the outset. The validity of the model may be judged not only by its physical reasoning but also by the comparison between the experimental and the numerical results. Unfortunately, in the case of cascade problems, very few experimental results are available. In the case of isolated foils, the pressure at the wake is known to quickly approach the pressure far downstream (Song 1963), and the calculation of cavity length beneath the free surface by Yim (1964) with Tulin's double spiral model matches very well with the experiments by Dawson and Bates (1962). Whether this is true in the case of cascades is yet to be found through experiments.

Although there is no numerical result for nonlinear theory available for a cascade of curved foils, yet the comparison between the linear and the nonlinear theory for flat plate cascades shows (in Figure 16) that, for large stagger angles, allowable solidities or angles of attack should be sufficiently small in order for the linear theory to be reasonably accurate in quantity. However in the case of cavitating high speed pumps, the stagger angles are naturally required to be large. Thus more coordination with experiments is required here.

Since the nonlinear theory for the supercavitating cascade with constant pressure cambered foil is not too difficult to solve, the higher order problem is being treated, and will be presented later.

REFERENCES

Acosta, A. J., "Cavitating Flow Past a Cascade of Circular Arc Hydrofoils," California Institute of Technology Hydrodynamics Laboratory Report No. E-79-2, March 1960.

Abbott, I. H., and Von Doenhoff, A.E., "Theory of Wing Sections," Dover Publication, New York, 1959.

Auslaender, J., "The Linearized Theory for Supercavitating Hydrofoils Operating at High Speeds Near a Free Surface," J. of Ship Research, Vol. 6, No. 2, October 1962.

Betz, A., and Petersohn, E., "Application of the Theory of Free Jets," NACA TN 667, April 1932.

Cohen, H., and Sutherland, C. D., "Finite Cavity Cascade Flow," Proceedings of the 3rd U. S. National Congress of Applied Mechanics, 1958.

Dawson, T. C., and Bates, B. R. Jr., "An Experimental Investigation of a Fully Cavitating Two-Dimensional Flat Plate Hydrofoil Near a Free Surface," Karman Laboratory of Fluid Mechanics and Jet Propulsion, California Institute of Technology Report No. E-118.12. October 1962.

Hsu, C. C., "Supercavitating Lifting Hydrofoils - Second Order Theory, HYDRONAUTICS, Incorporated Technical Report 121-6, March 1966.

Jakobsen, J. K., "Supercavitating Cascade Flow Analysis," Paper No. 64-FE-11, ASME, 1964.

Johnson, V.E., and Starley, S., "The Design of Base-Vented Struts for High Speed Hydrofoil Systems," The Proceedings of a Symposium on Air Cushion Vehicles and Hydrofoils, I.A.S., August 1962.

Muskhelishvili, N.I., "Singular Integral Equations," P. Noordhoff N.V. Groningen-Holland, 1953.

Sedov, L. L., "Two Dimensional Problems in Hydrodynamics and Aerodynamics," pp. 110-126. Interscience Publishers 1965.

Song, C. S., "Two-Dimensional Supercavitating Plate Oscillating Under a Free-Surface," University of Minnesota, St. Anthony Falls Hydraulic Laboratory, Technical Report No. 47, Series B., December 1963.

Stripling, L. B., and Acosta, A. J., "Cavitation in Turbo-Pumps - Part 1," J. of Basic Engineering, Series D., Vol. 84, pp. 326-338, 1962.

Tulin, M. P., "Steady Two-Dimensional Cavity Flows About Slender Bodies," D.T.M.B. Report 834, May 1953.

Tulin, M.P., and Burkart, M. P., "Linearized Theory for Flows About Lifting Foils at Zero Cavitation Number, D.T.M.B. Report C-638, February 1955.

Tulin, M. P., "Supercavitating Flows - Small Perturbation Theory," Journal of Ship Research, Vol. 7, No. 3, 1964.

Wade, R. B., "Flow Past a Partially Cavitating Cascade of Flat Plate Hydrofoils," California Institute of Technology Hydrodynamics Laboratory Report No. E-79.4, January 1963.

Wade, R. B., and Acosta, "Investigation of Cavitating Cascades," Paper No. 66-WA/FE-25, ASME, 1967.

Yim, B., "On Finite Length Cavities Beneath a Free Surface," HYDRONAUTICS, Incorporated Technical Report 119-4, December 1962.

Yim, B., "On a Fully Cavitating Two-Dimensional Flat Plate Hydrofoil with Non-Zero Cavitation Number Near a Free Surface," HYDRONAUTICS, Incorporated Technical Report 463-4, June 1964.

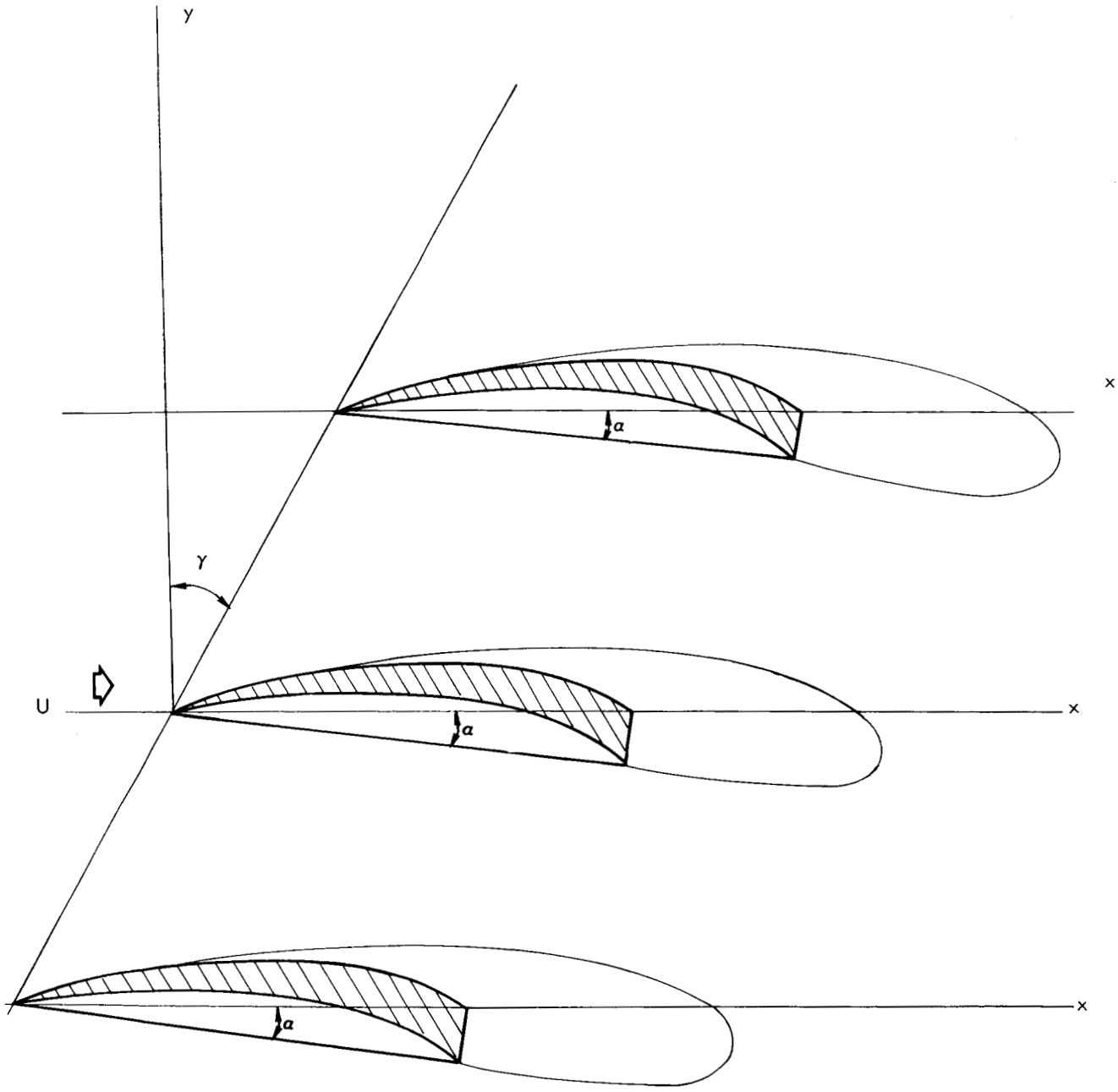

FIGURE 1a - Z PLANE (NON LINEAR)

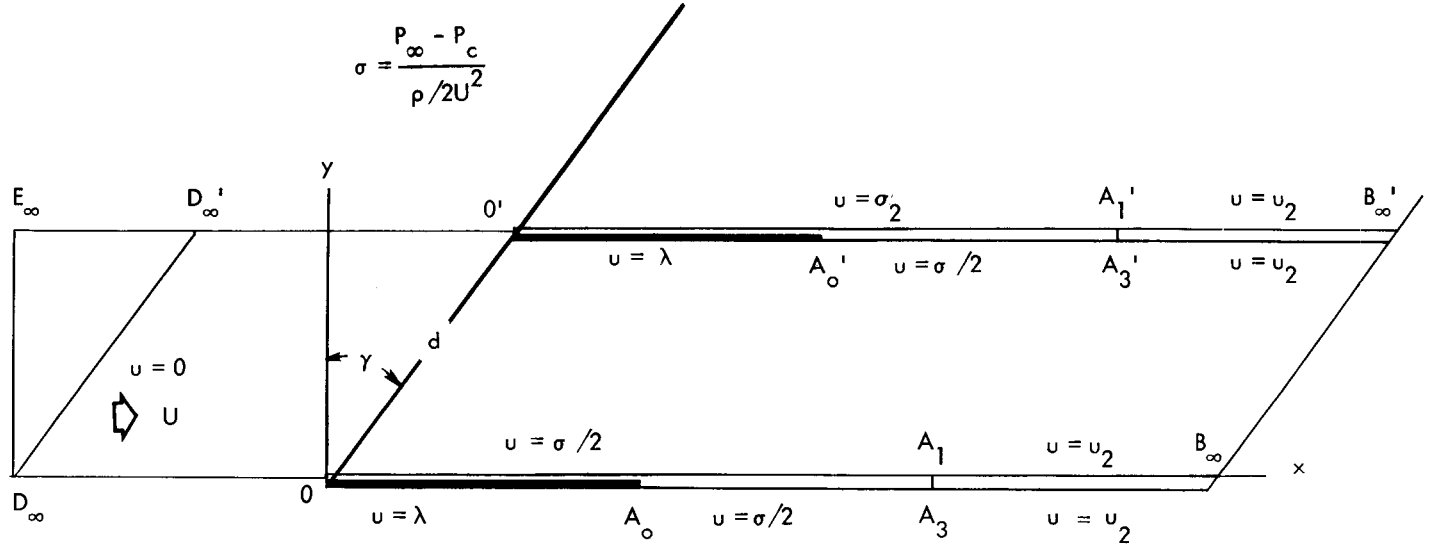

FIGURE 1b - Z PLANE (LINEAR)

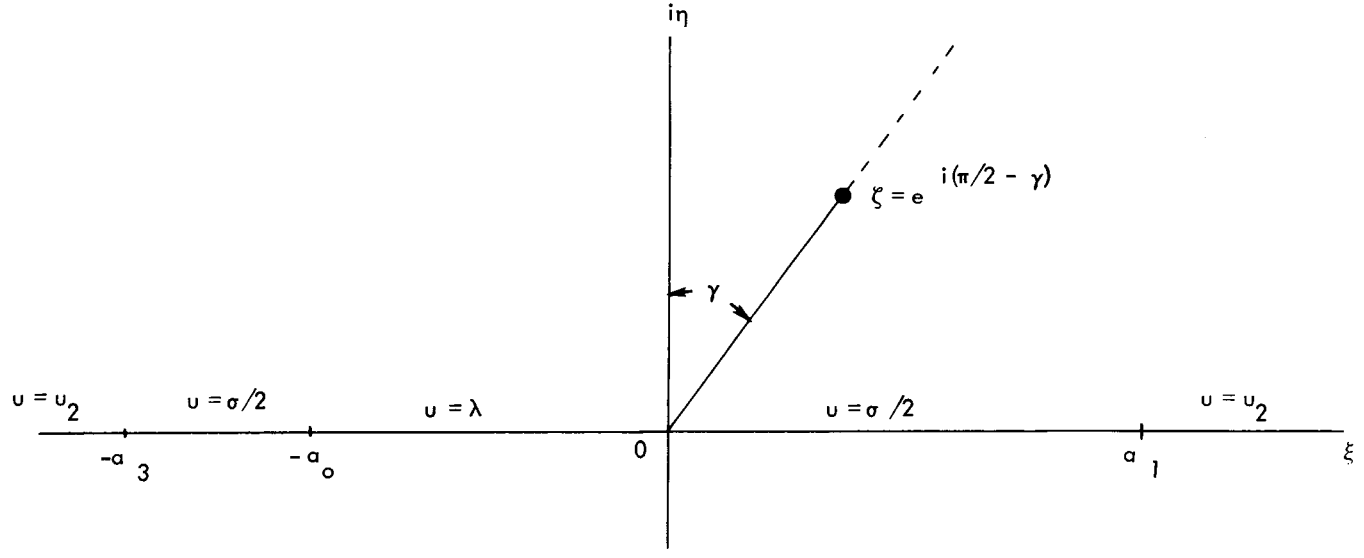

FIGURE 1c - ζ PLANE

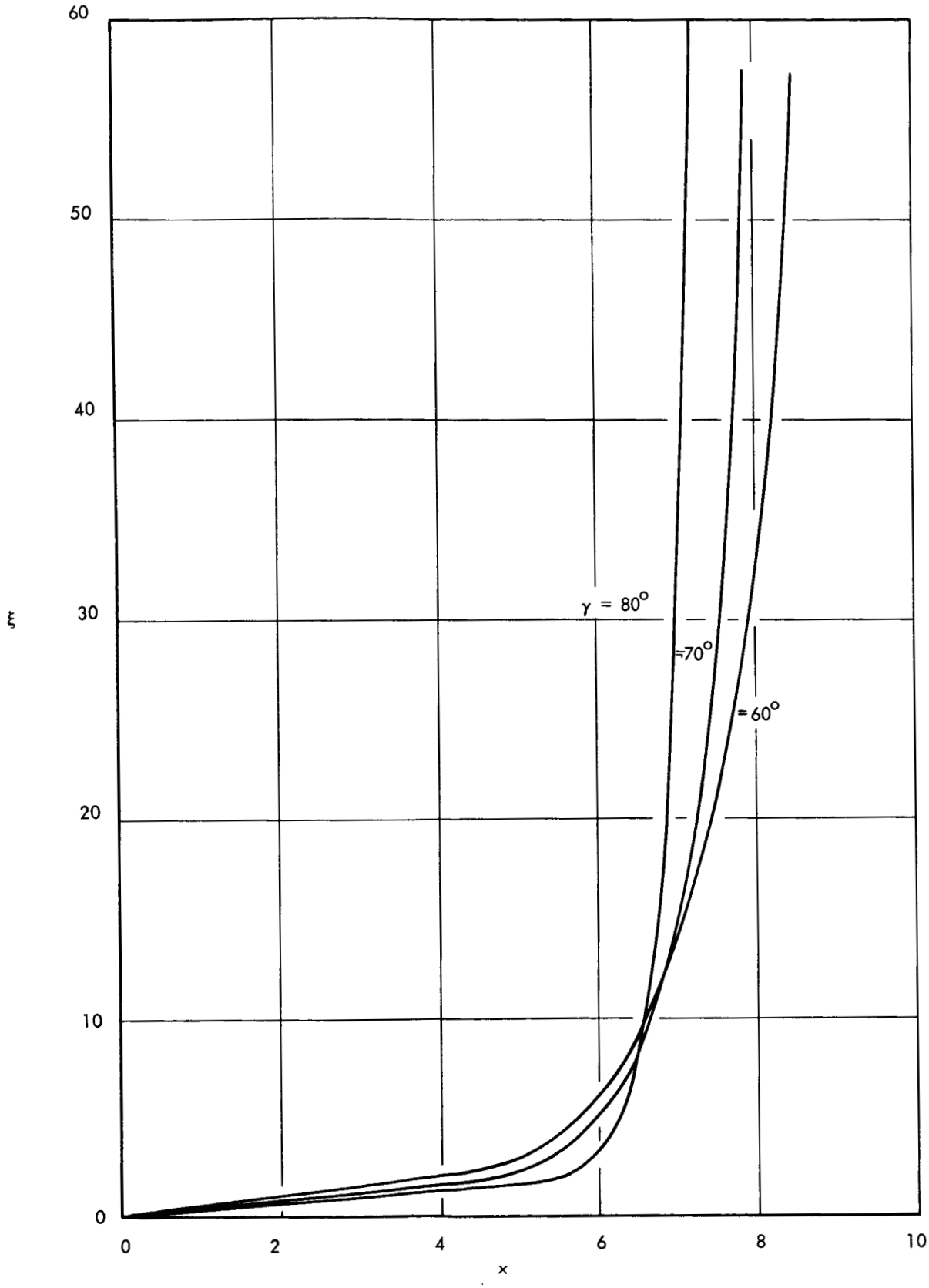

FIGURE 2a - RELATIONS BETWEEN PHYSICAL COORDINATES (x, y) AND TRANSFORMED COORDINATES (ξ, η)

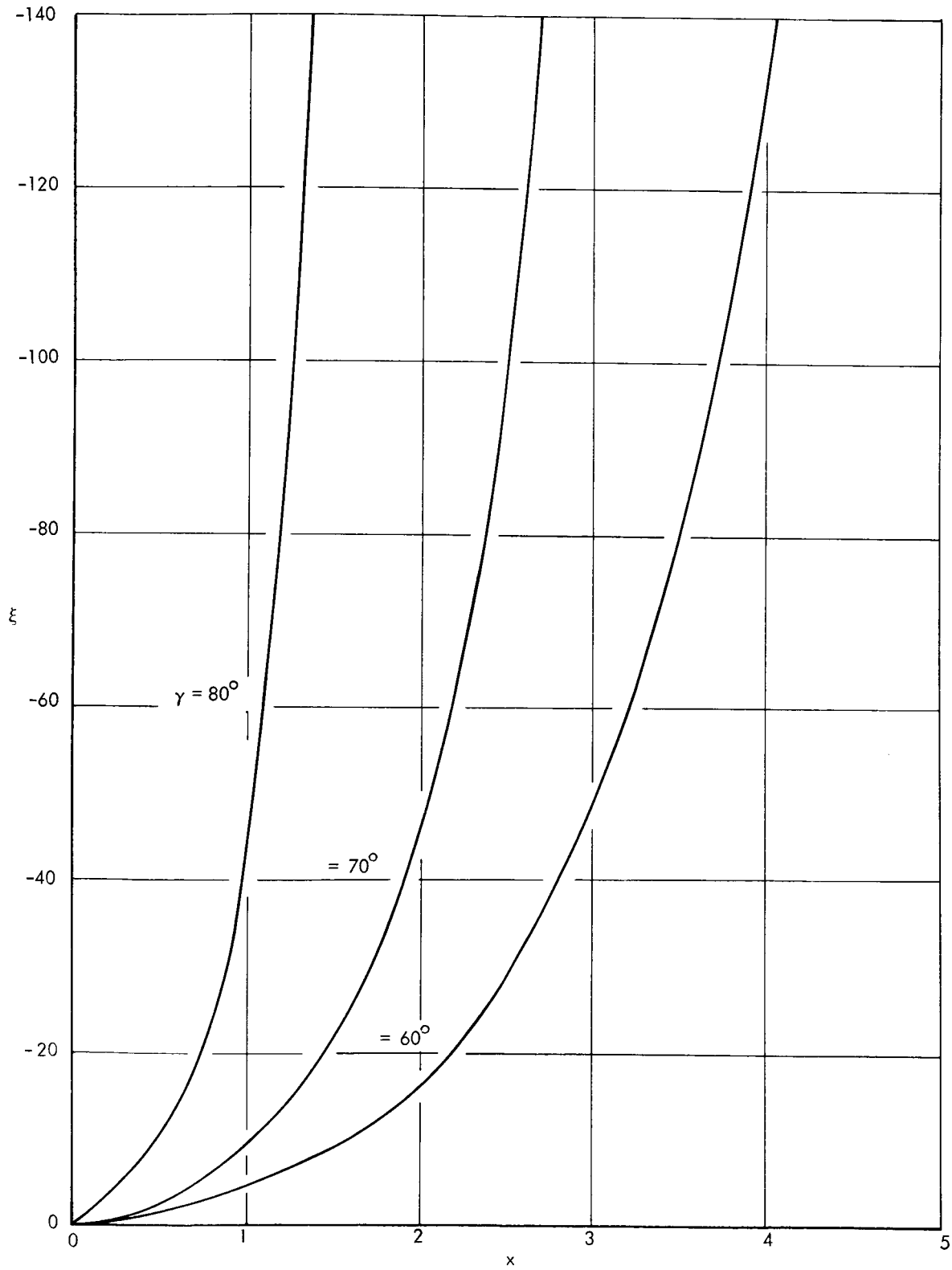

FIGURE 2b - RELATIONS BETWEEN PHYSICAL COORDINATES (x, y) AND TRANSFORMED COORDINATES (ξ, η)

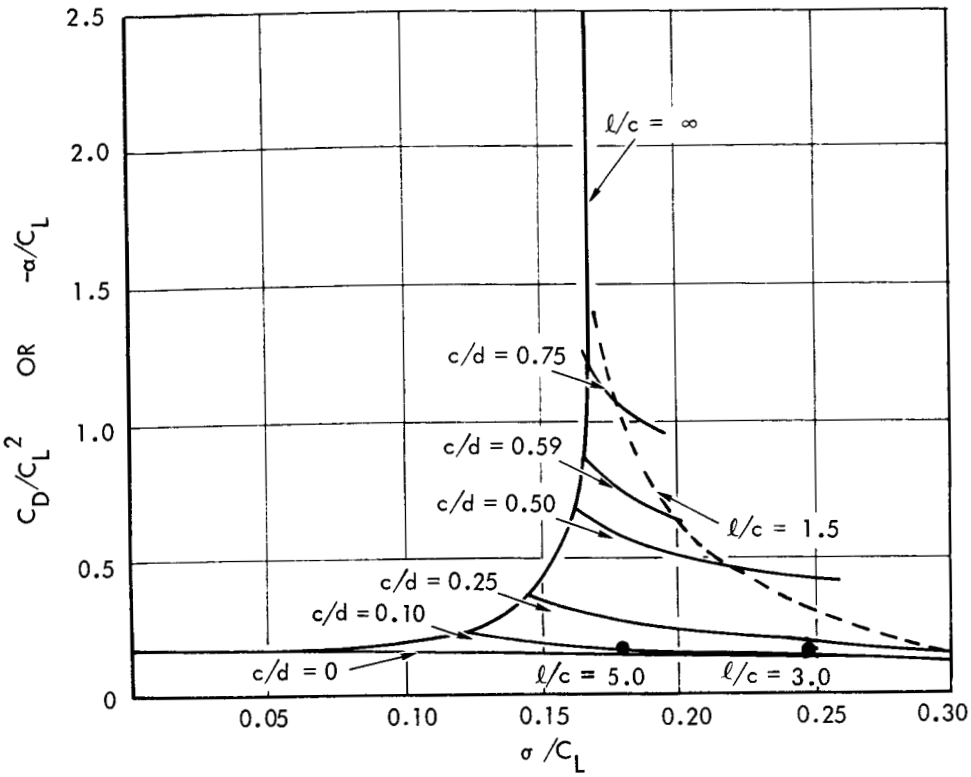

FIGURE 3 - RELATIONS BETWEEN DRAG COEFFICIENTS, LIFT COEFFICIENTS, AND CAVITATION NUMBERS OF SUPERCAVITATING CASCADES WITH A STAGGER ANGLE OF 60 DEGREES

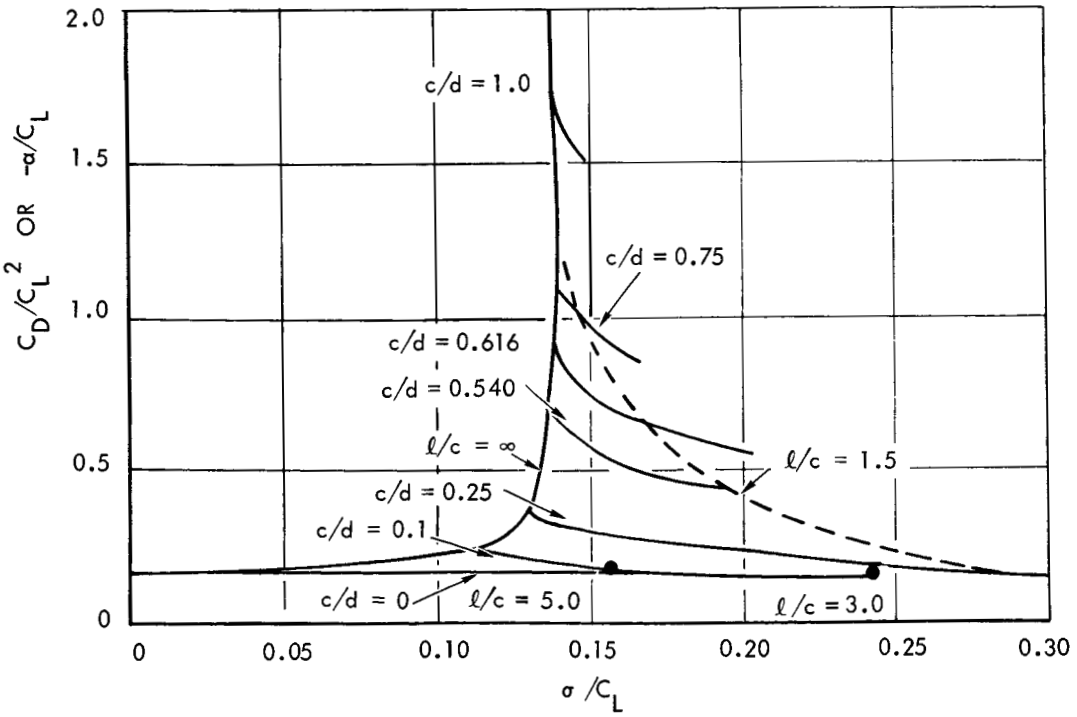

FIGURE 4 - RELATIONS BETWEEN DRAG COEFFICIENTS, LIFT COEFFICIENTS, AND CAVITATION NUMBERS OF SUPERCAVITATING CASCADES WITH A STAGGER ANGLE OF 65 DEGREES

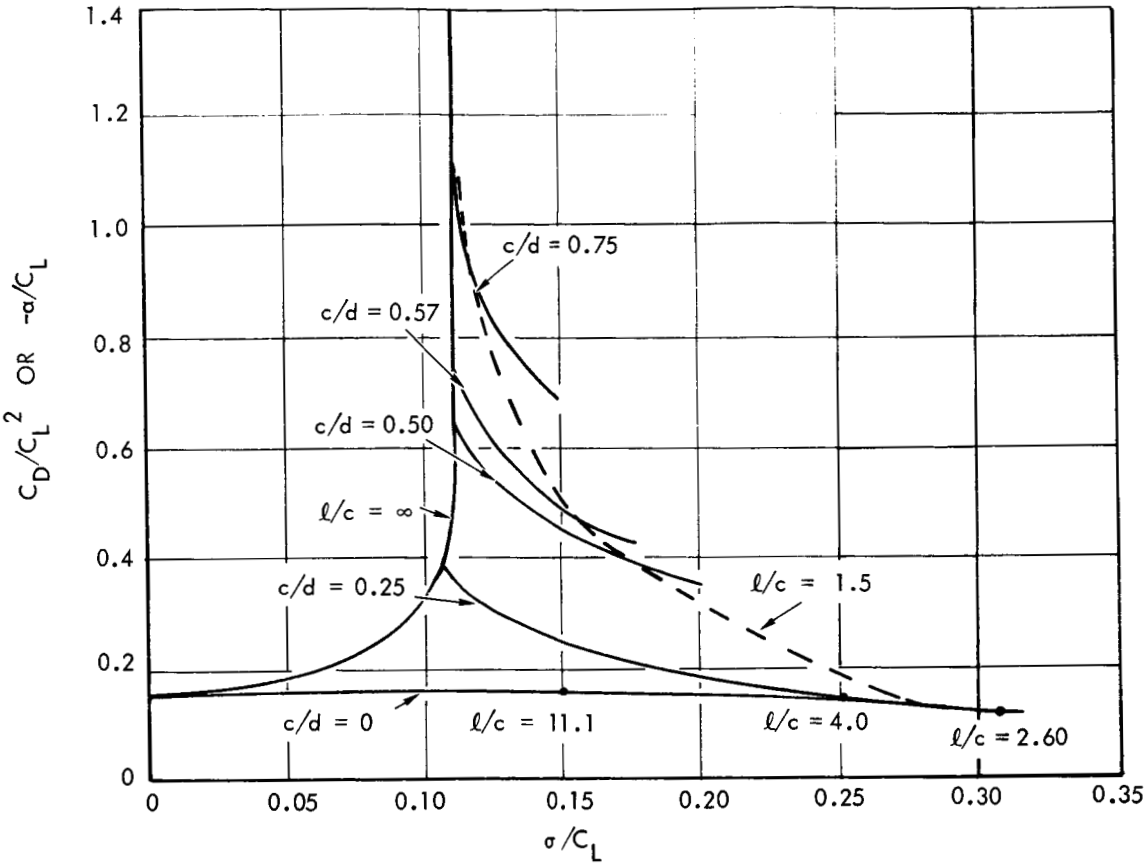

FIGURE 5 - RELATIONS BETWEEN DRAG COEFFICIENTS, LIFT COEFFICIENTS, AND CAVITATION NUMBERS OF SUPERCAVITATING CASCADES WITH A STAGGER ANGLE OF 70 DEGREES

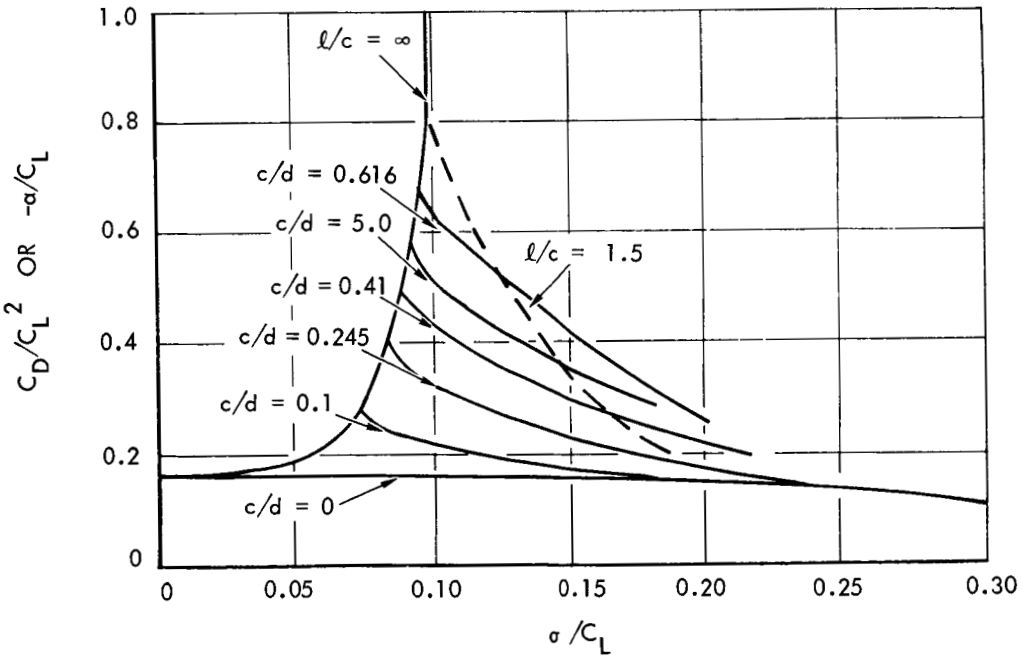

FIGURE 6 - RELATIONS BETWEEN DRAG COEFFICIENTS, LIFT COEFFICIENTS, AND CAVITATION NUMBERS OF SUPERCAVITATING CASCADES WITH A STAGGER ANGLE OF 75 DEGREES

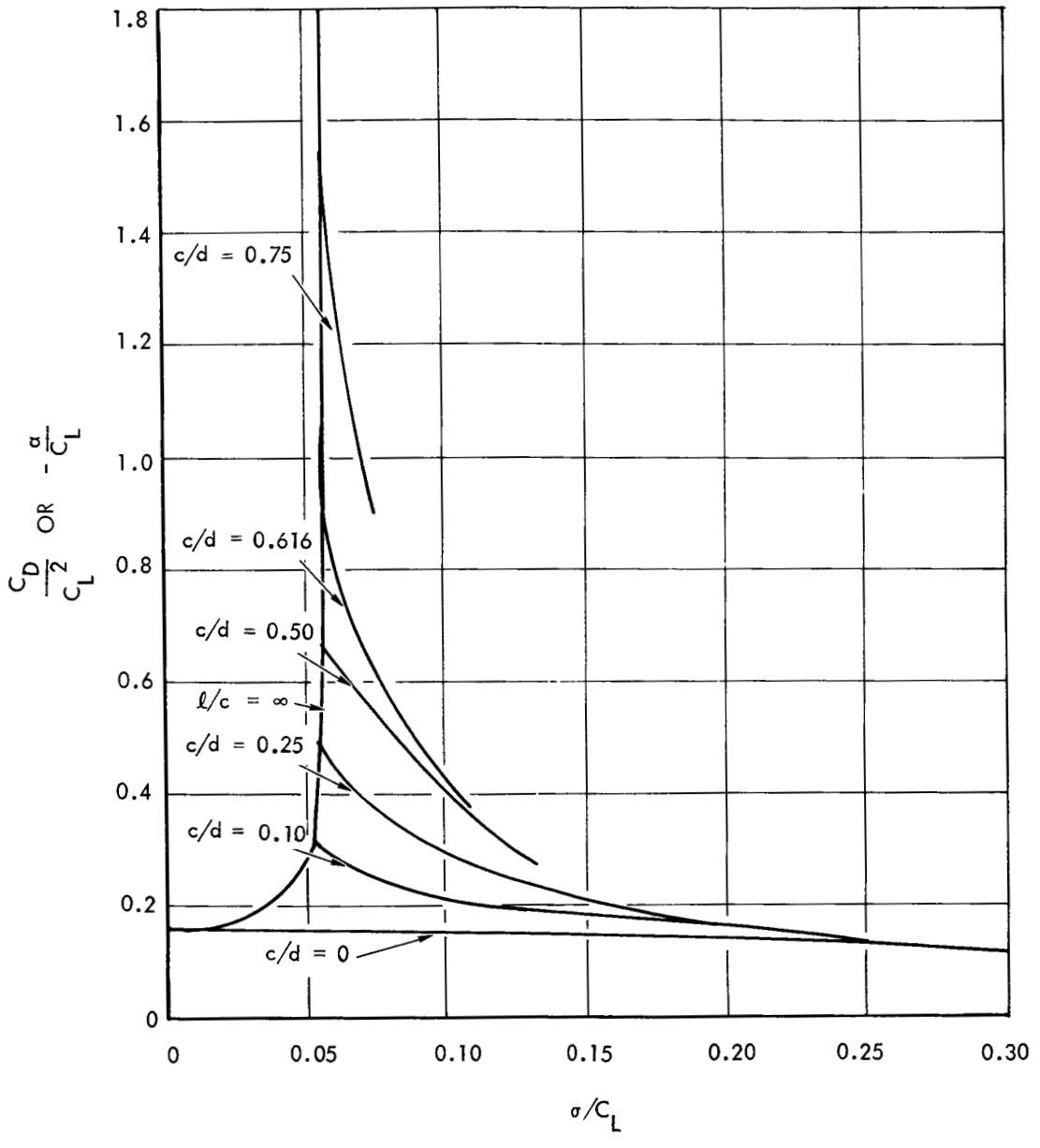

FIGURE 7 - RELATIONS BETWEEN DRAG COEFFICIENTS, LIFT COEFFICIENTS, AND CAVITATION NUMBERS OF SUPERCAVITATING CASCADES WITH A STAGGER ANGLE OF 80°

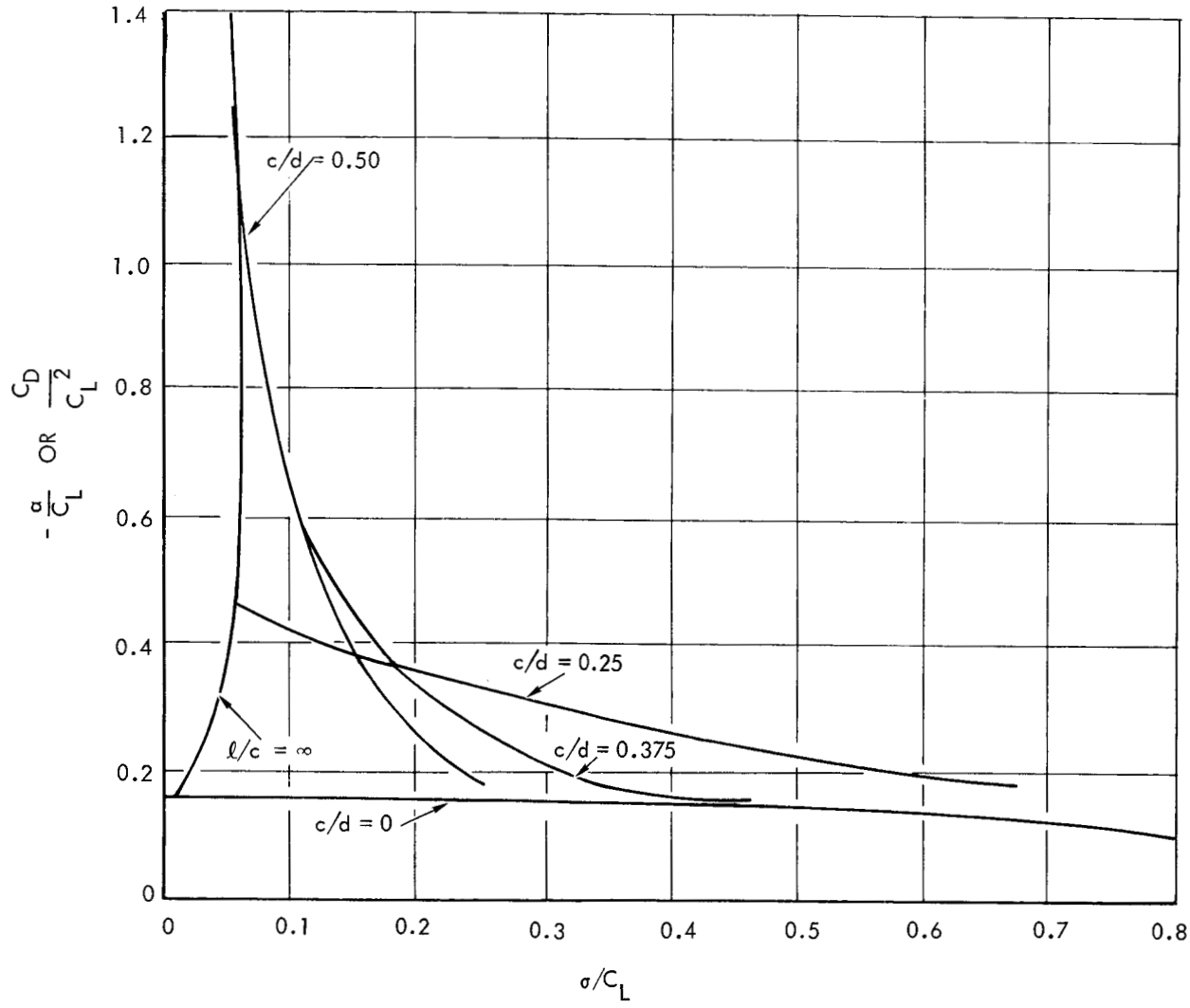

FIGURE 8 - RELATIONS BETWEEN DRAG COEFFICIENTS, LIFT COEFFICIENTS, AND CAVITATION NUMBERS OF SUPERCAVITATING CASCADES WITH A STAGGER ANGLE OF 85 DEGREES

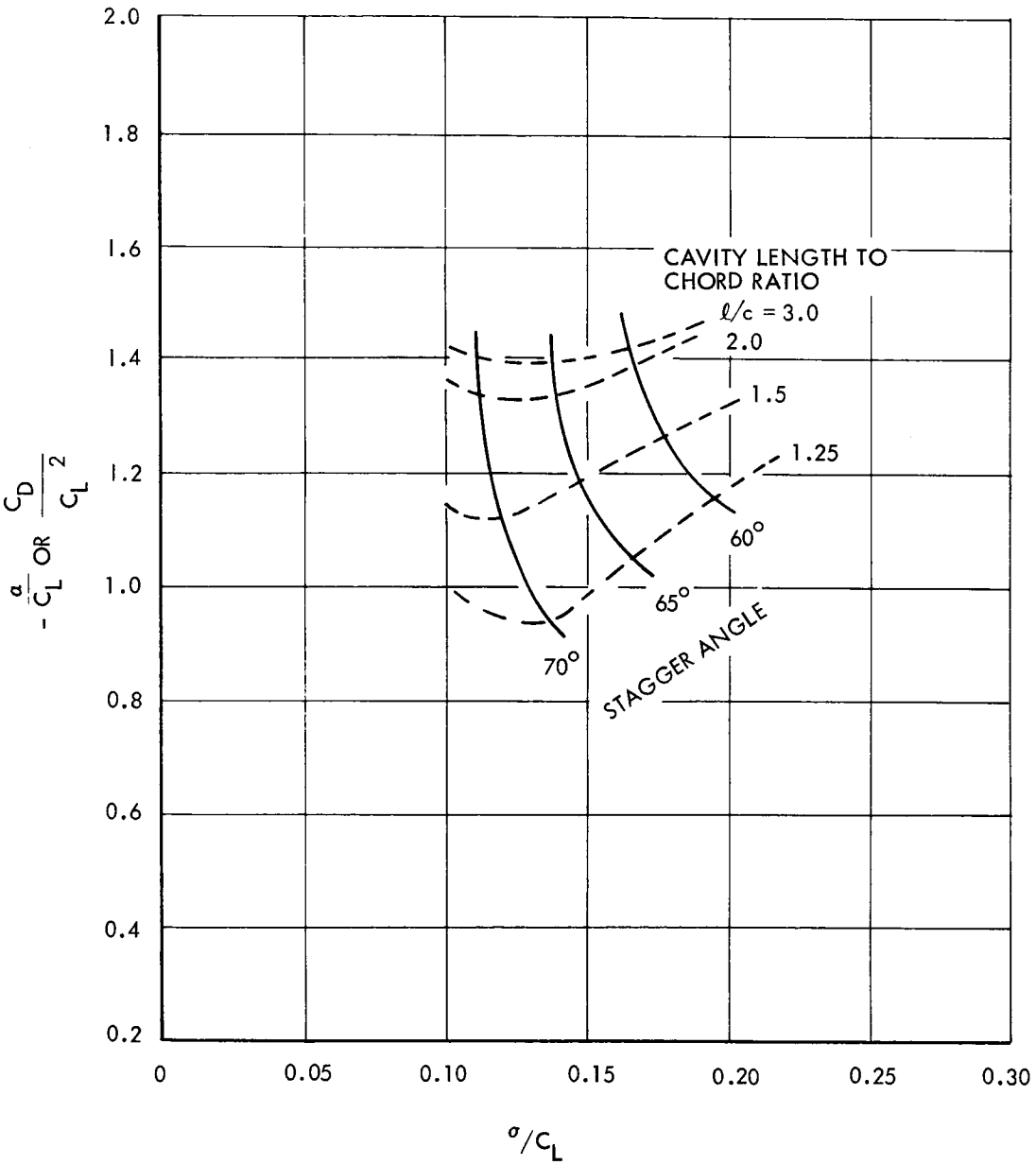

FIGURE 9 - RELATIONS BETWEEN DRAG COEFFICIENTS, LIFT COEFFICIENTS, AND CAVITATION NUMBERS OF SUPERCAVITATING CASCADES WITH A SOLIDITY OF 0.75

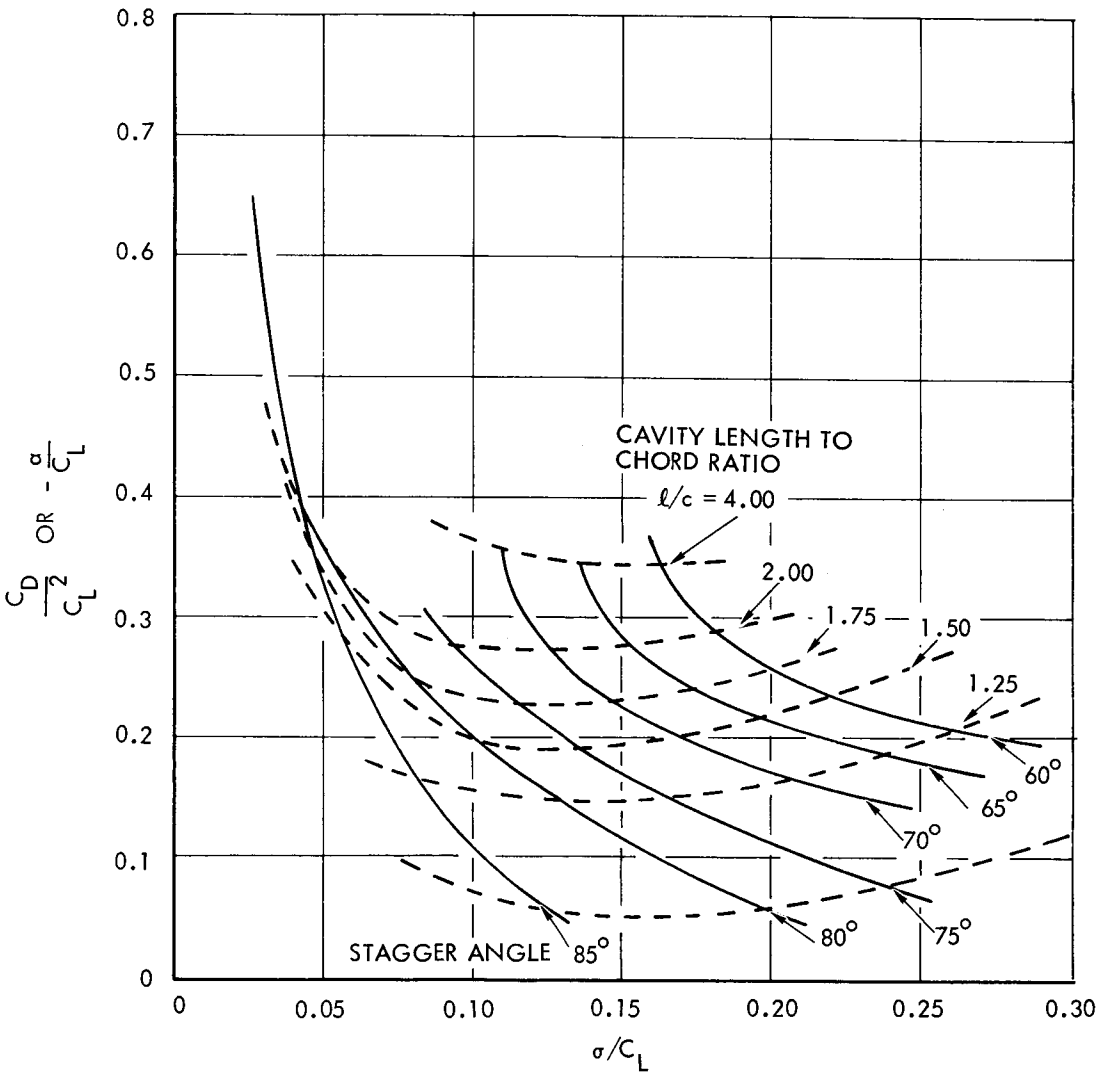

FIGURE 10 - RELATIONS BETWEEN DRAG COEFFICIENTS, LIFT COEFFICIENTS AND CAVITATION NUMBERS OF SUPERCAVITATING CASCADES WITH SOLIDITY OF 0.50

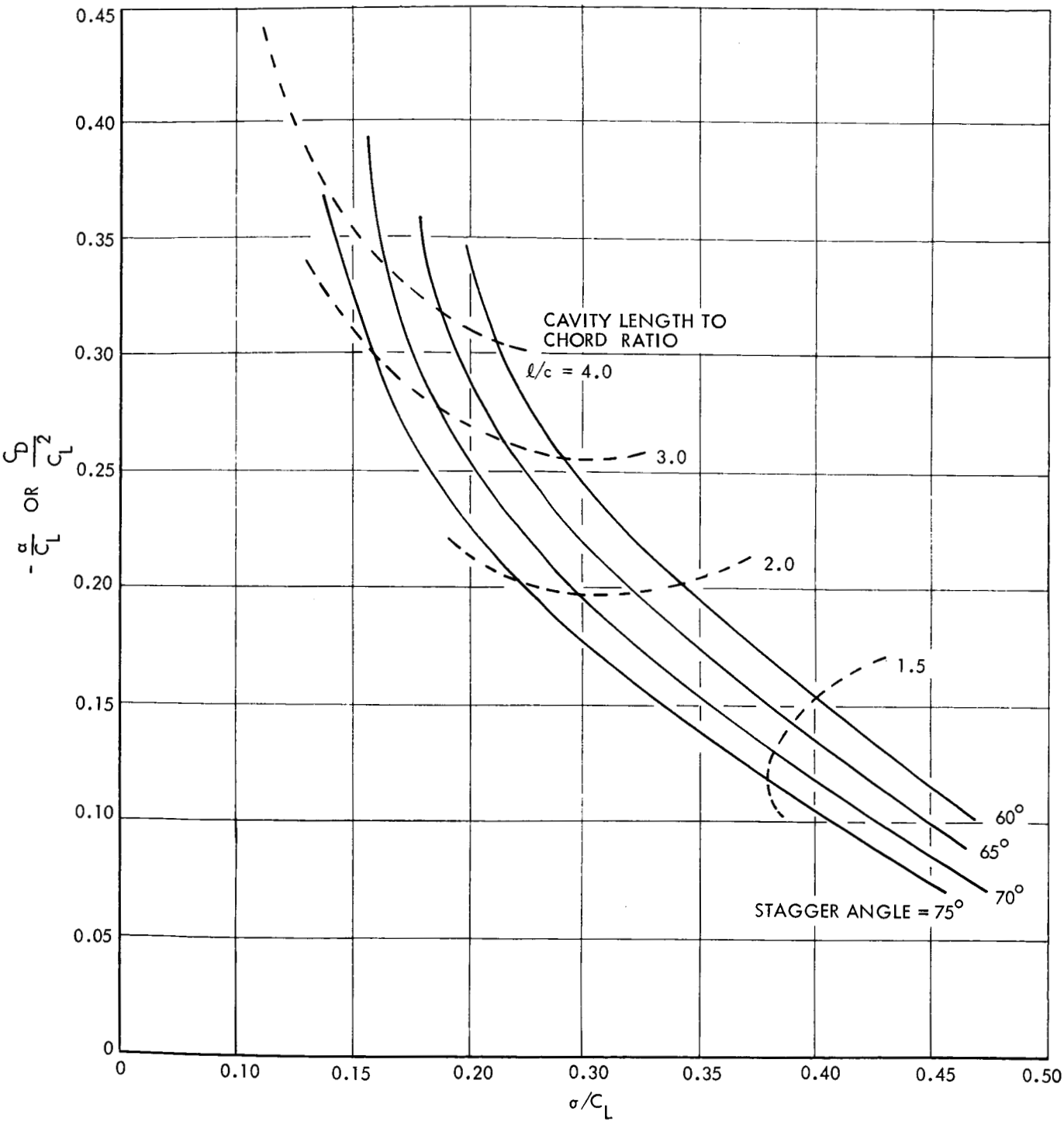

FIGURE 11 - RELATIONS BETWEEN DRAG COEFFICIENTS, LIFT COEFFICIENTS, AND CAVITATION NUMBERS OF SUPERCAVITATING CASCADES WITH A SOLIDITY OF 0.25

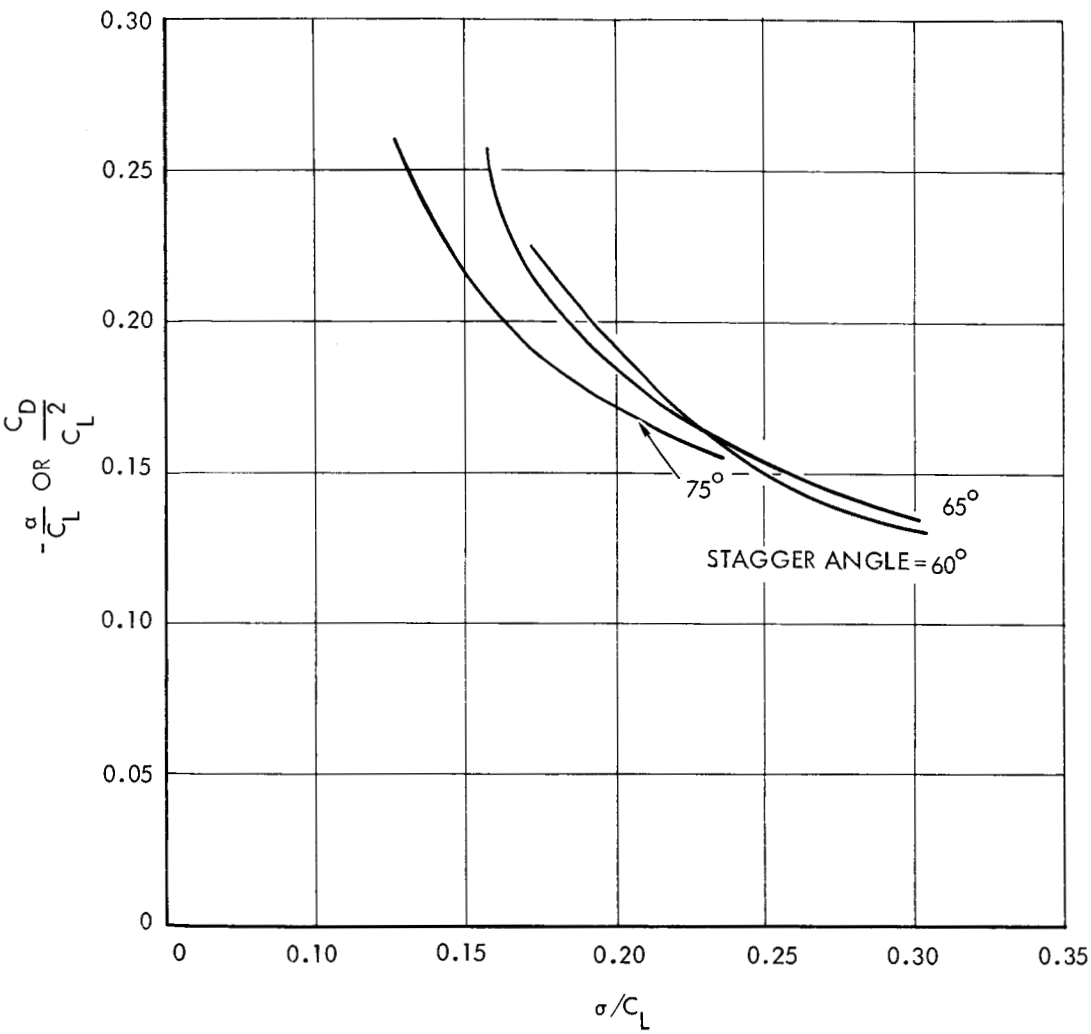

FIGURE 12 - RELATIONS BETWEEN DRAG COEFFICIENTS, LIFT COEFFICIENTS, AND CAVITATION NUMBERS OF SUPERCAVITATING CASCADES WITH A SOLIDITY OF 0.10

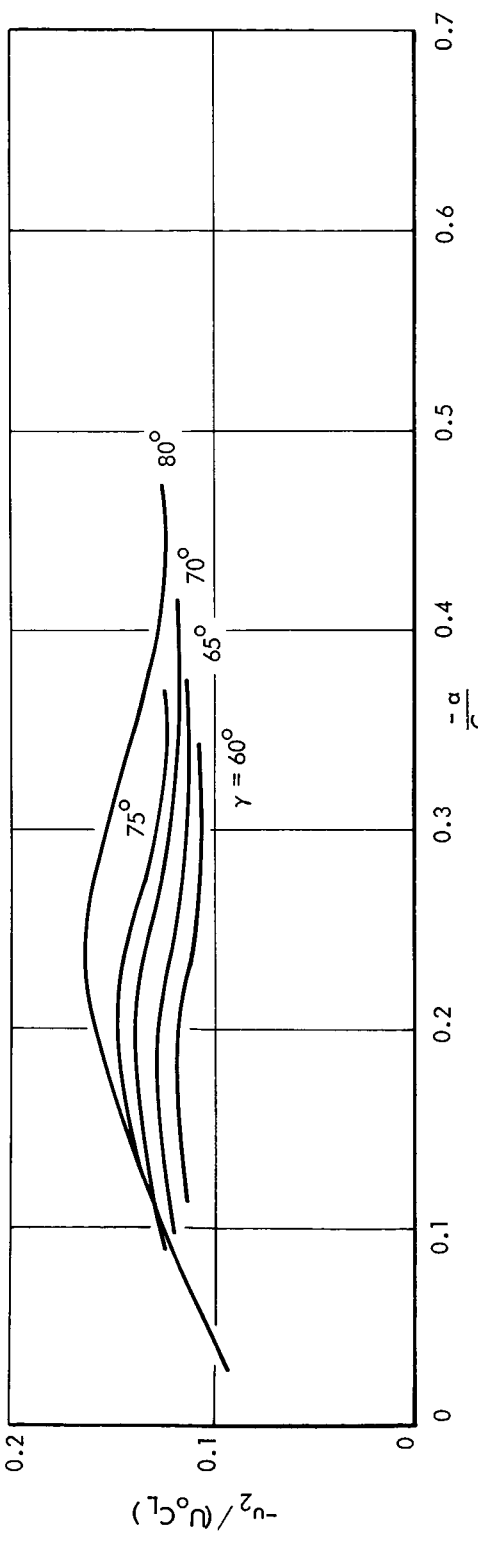

FIGURE 13 - x COMPONENT OF PERTURBATION VELOCITY AT $x = \infty$ VERSUS ANGLE OF ATTACK FOR SUPERCAVITATING CASCADES WITH FINITE CAVITIES AT A SOLIDITY OF 0.25

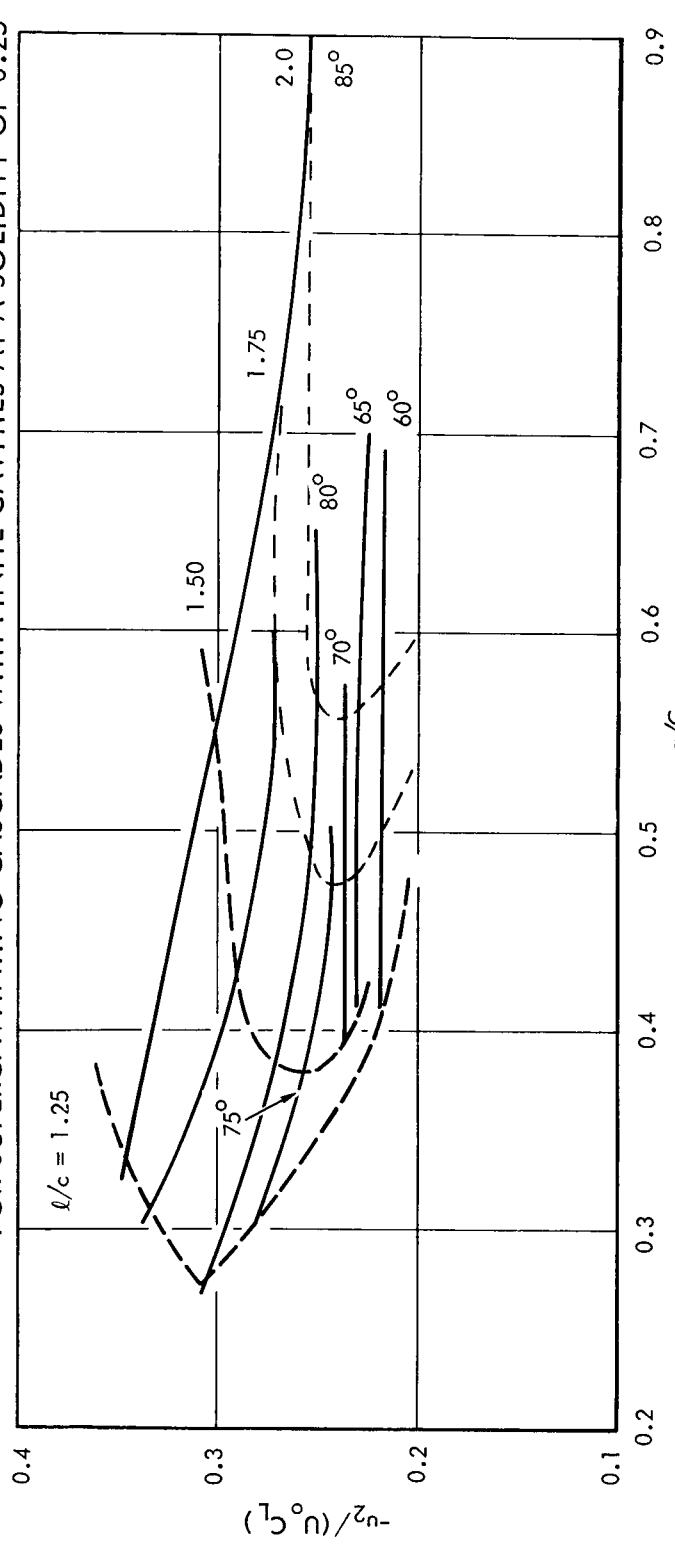

FIGURE 14 - x COMPONENT OF PERTURBATION VELOCITY AT $x = \infty$ VERSUS ANGLE OF ATTACK FOR SUPERCAVITATING CASCADES WITH FINITE CAVITIES AT A SOLIDITY OF 0.50

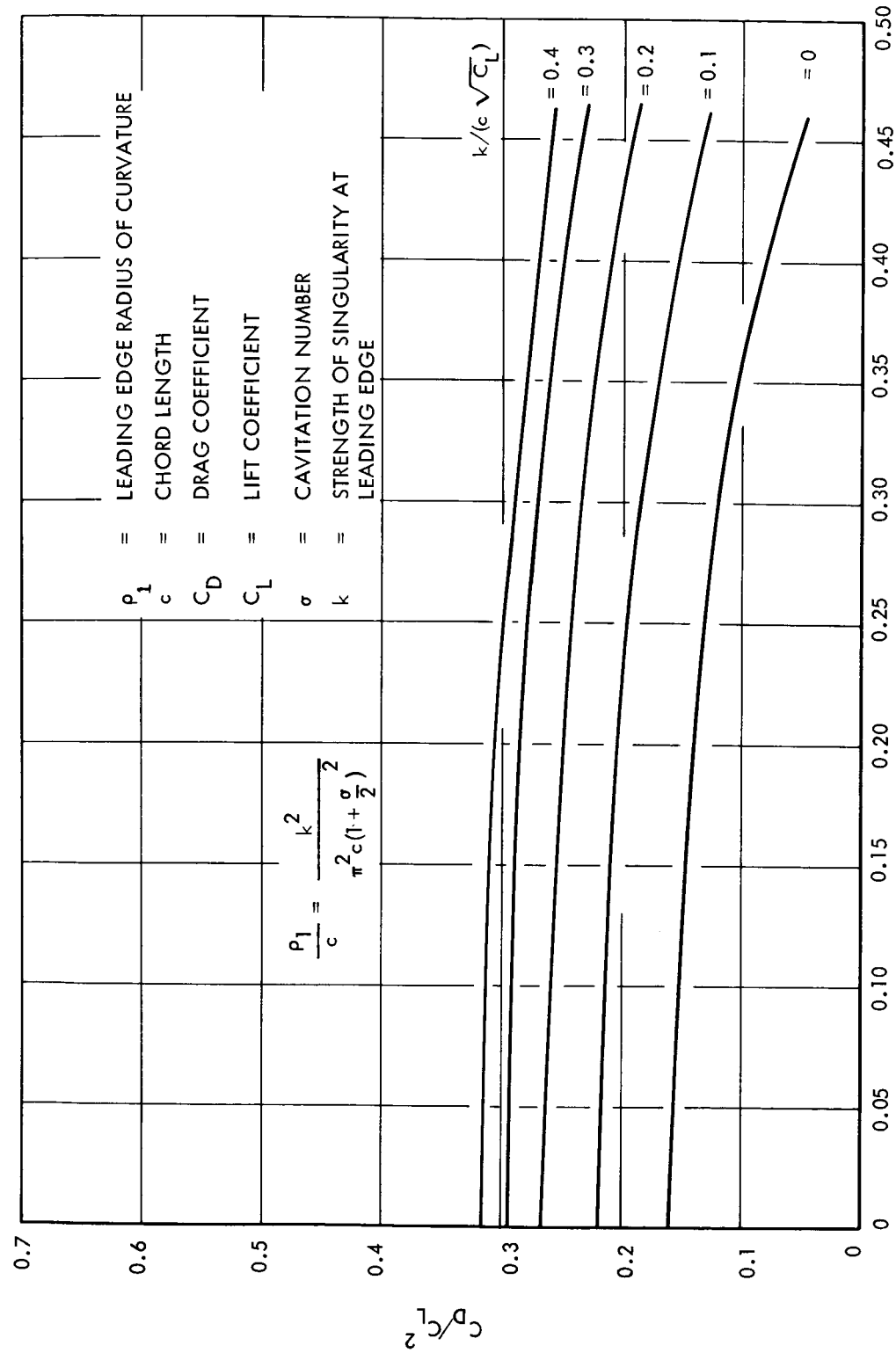

FIGURE 15 - INFLUENCE OF LEADING EDGE CURVATURE ON AN ISOLATED CONSTANT-PRESSURE CAMBER HYDROFOIL

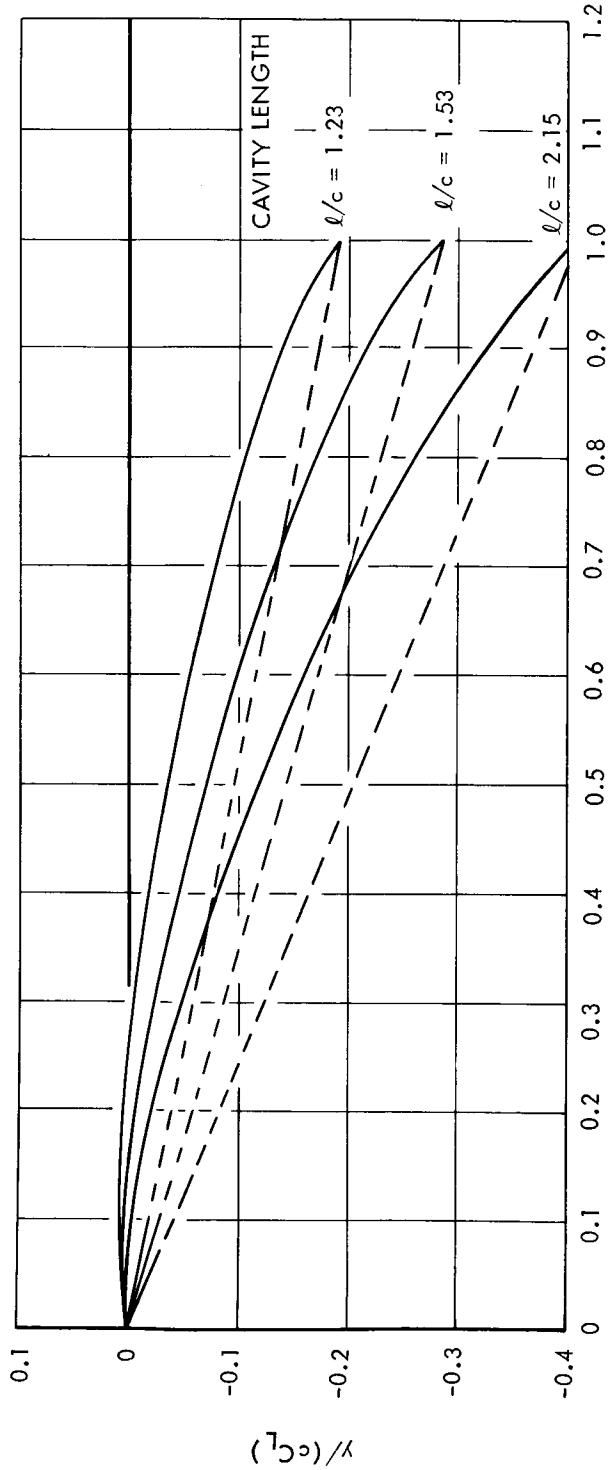

FIGURE 16 - SHAPE OF CONSTANT-PRESSURE CAMBERED FOILS IN A SUPERCAVITATING CASCADE WITH A STAGGER ANGLE OF 75° AND A SOLIDITY OF 0.407

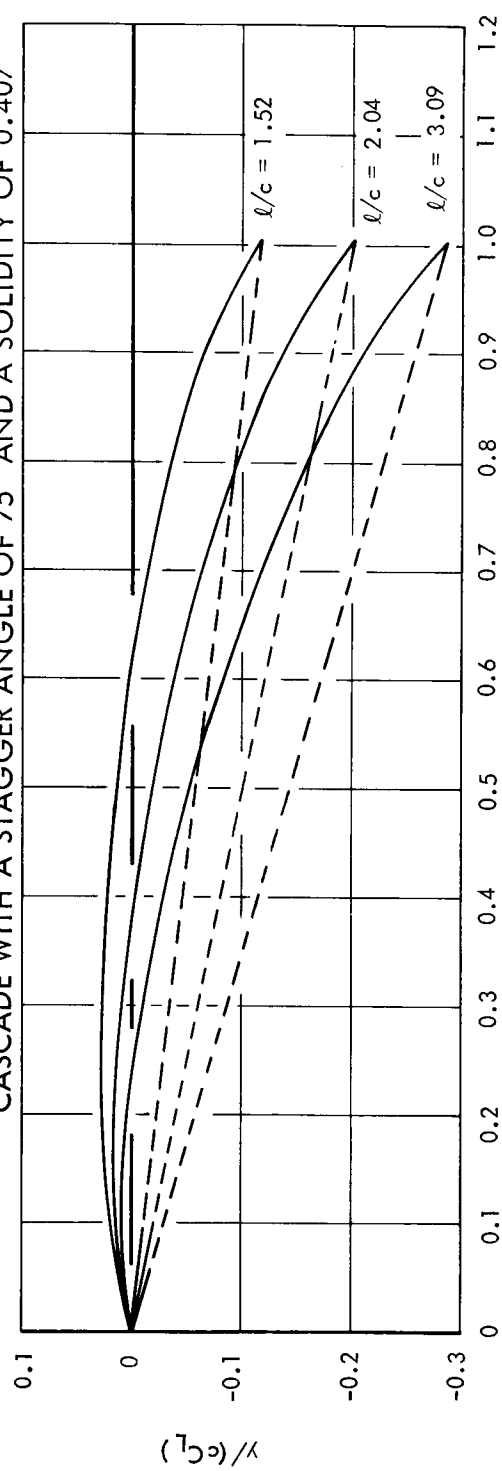

FIGURE 17 - SHAPE OF CONSTANT-PRESSURE CAMBERED FOILS IN A SUPERCAVITATING CASCADE WITH A STAGGER ANGLE OF 75° AND A SOLIDITY OF 0.245

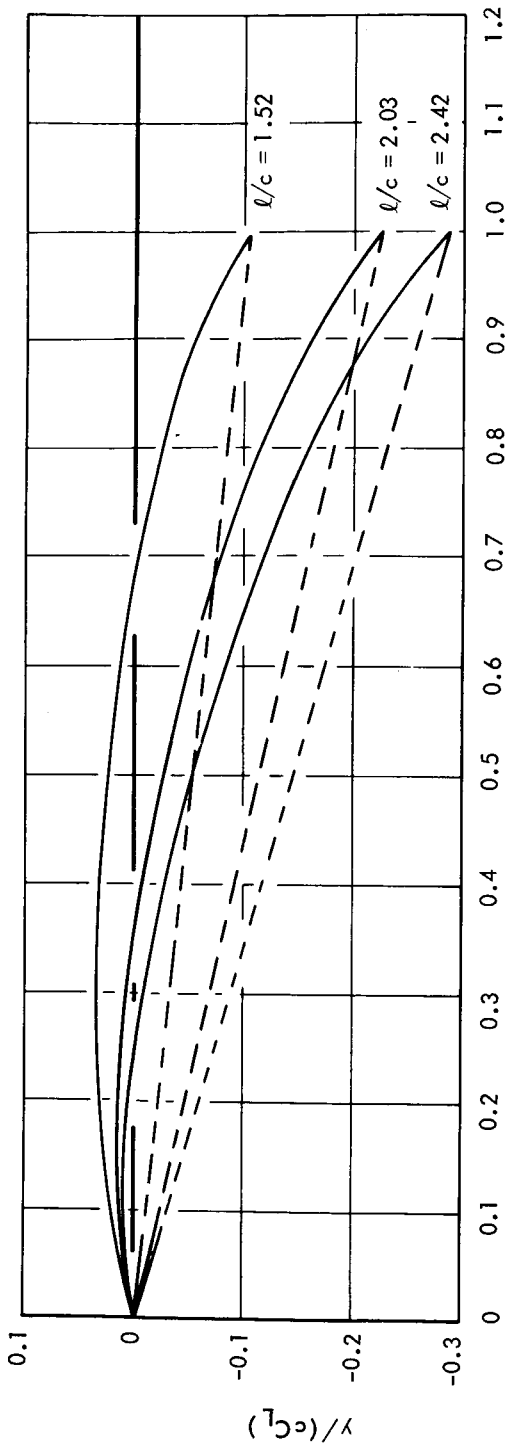

FIGURE 18 - SHAPE OF CONSTANT-PRESSURE CAMBERED FOILS IN A SUPERCAVITATING CASCADE WITH A STAGGER ANGLE OF 80 DEGREES AND A SOLIDITY OF 0.246

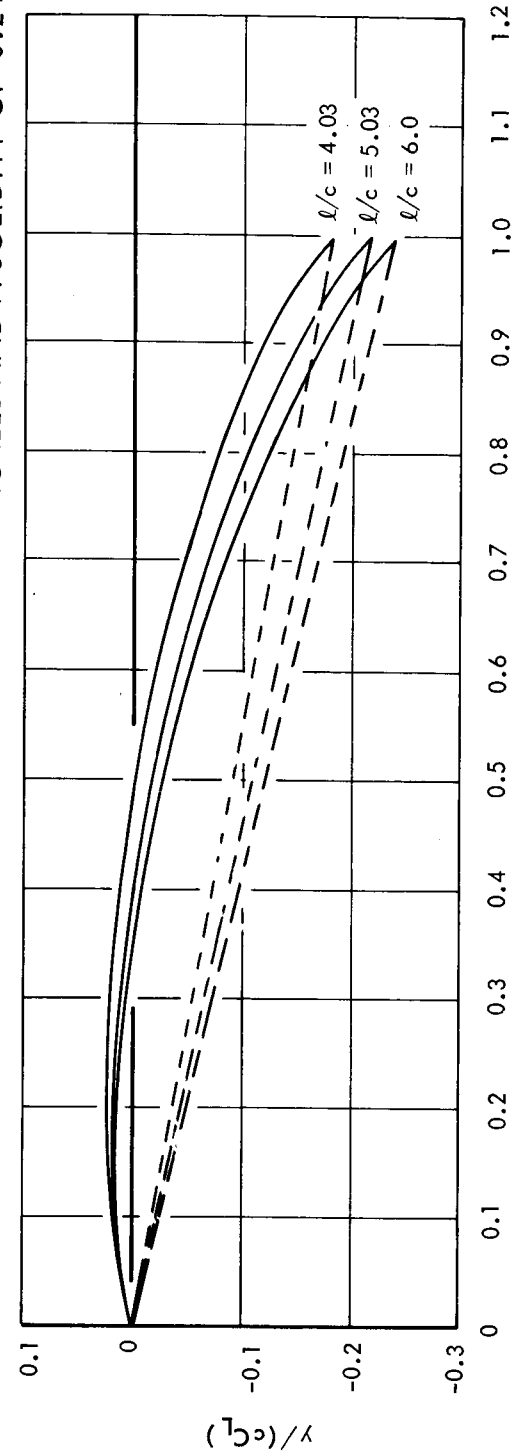

FIGURE 19 - SHAPE OF CONSTANT-PRESSURE CAMBERED FOILS IN A SUPERCAVITATING CASCADE WITH A STAGGER ANGLE OF 80 DEGREES AND A SOLIDITY OF 0.10

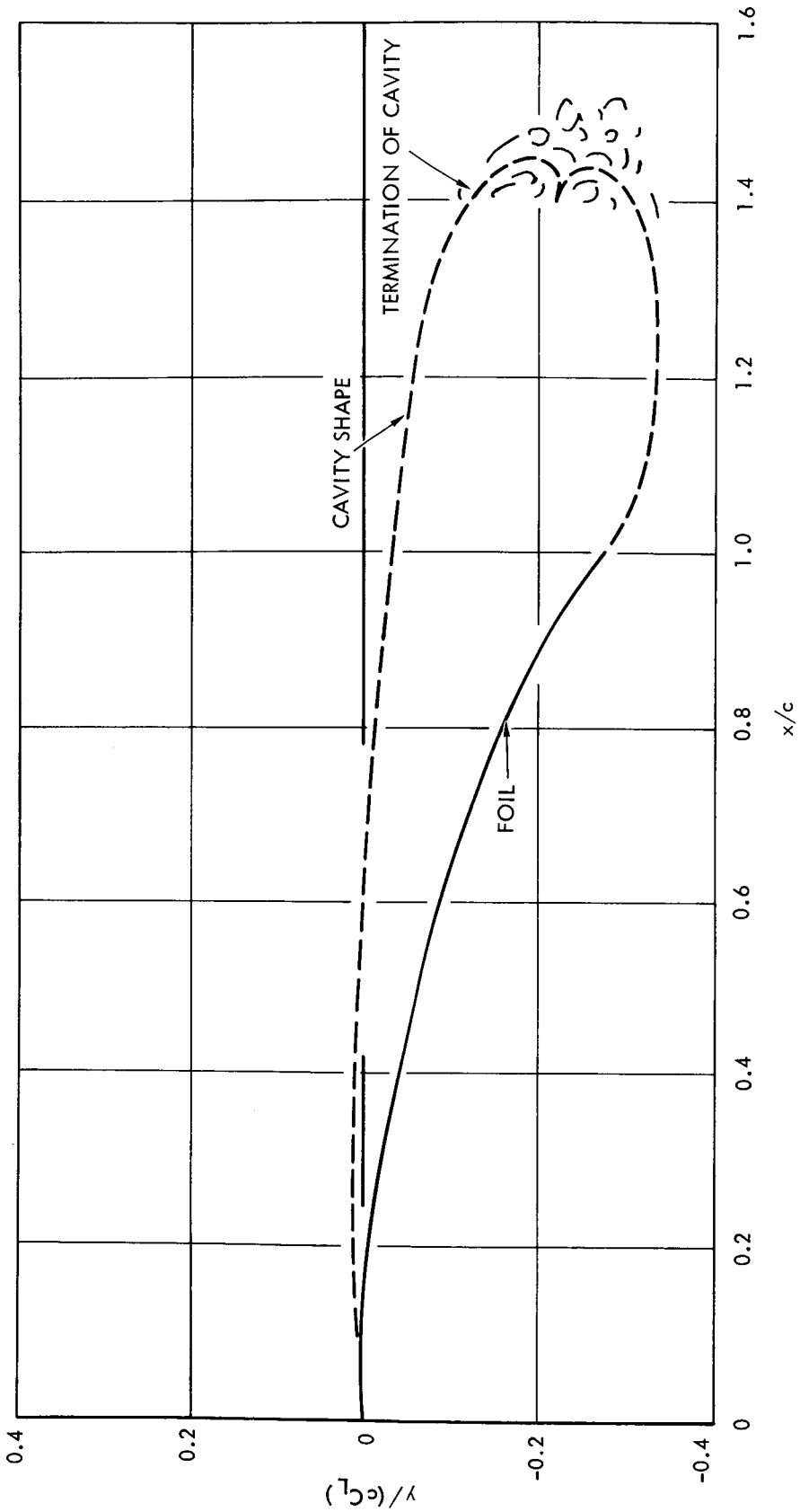

FIGURE 20 - TYPICAL FOIL AND RESULTING CAVITY SHAPE FOR SHOCK FREE ENTRY - STAGGER ANGLE = 80 DEGREES, $c/d = 0.41$, $\ell/c = 1.45$, $\sigma/C_L = 0.13$

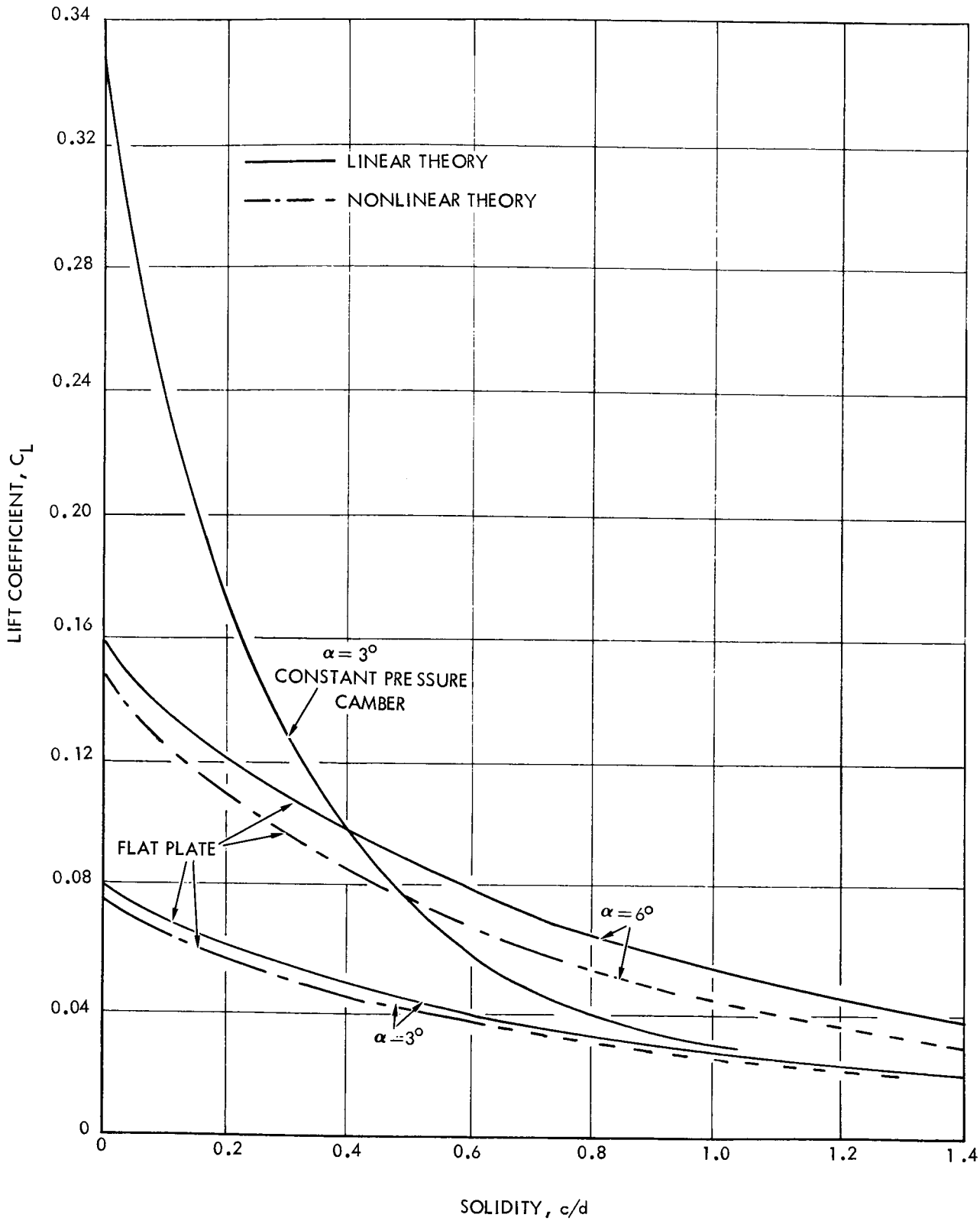

FIGURE 21 - LIFT COEFFICIENT VS SOLIDITY OF CASCADES STAGGER ANGLE, 60°
CAVITY LENGTH = ∞

HYDRONAUTICS, Incorporated

DISTRIBUTION LIST
(Contract NAS 8-20625)

NASA Marshall Space Flight Center
Huntsville, Alabama 35812
Attn: Office of Technical Information, MS-IP 2
Technical Library 1
Keith Chandler 1
Technology Utilization Office, MS-T 1
R-P and VE-P, H. F. Beduerftig 2

Chief, Liquid Propulsion Technology, RPL
Office of Advanced Research and Technology
NASA Headquarters
Washington, D. C. 20546 4

NASA Scientific and Technical Information Facility
P. O. Box 33
College Park, Maryland 20740 25

Mr. Vincent L. Johnson
Director, Launch Vehicles and Propulsion, SV
Office of Space Science and Applications
NASA Headquarters,
Washington, D. C. 20546 1

Jet Propulsion Laboratory
California Institute of Technology
4800 Oak Grove Drive
Pasadena, California 91103
Attn: Henry Burlage, Jr. 1
Propulsion Div., 38 1

Langley Research Center
Langley Station
Hampton, Virginia 23365
Attn: Dr. Floyd L. Thompson
Director 2

Lewis Research Center
21000 Brookpark Road
Cleveland, Ohio 44135
Attn: Ambrose Ginsburg 2

Marshall Space Flight Center
Huntsville, Alabama 38812
Attn: Hans G. Paul 1
Code R-Pand VE-P 1

Air Force Rocket Propulsion Laboratory
Research and Technology Div.
Air Force Systems Command
Edwards, California 93523
Attn: RPRR/Mr. H. Main 1

Aerojet-General Corporation
P. O. Box 1947
Technical Library, Bldg. 2015, Dept. 2410
Sacramento, California 95809
Attn: R. Stiff 1

Beech Aircraft Corporation
Boulder Facility
Box 631
Boulder, Colorado
Attn: J. H. Rodgers 1

Bell Aerosystems Company
P. O. Box 1
Buffalo 5, N. Y.
Attn: W. M. Smith 1

Advanced Engine and Technology Dept.
General Electric Company
Cincinnati, Ohio 45215
Attn: D. Suichu 1

Florida Res. and Dev. Center
Pratt and Whitney Aircraft
United Aircraft Corporation
P.O. Box 2691
West Palm Beach, Florida 33402
Attn: R. J. Coar 1

Reaction Motors Division
Thiokol Chemical Corporation
Denville, New Jersey 07832
Attn: Arthur Sherman 1

Rocketdyne (Library Dept. 586-306) Div. of North American Aviation
6633 Canoga Avenue
Canoga Park, California 91304
Attn: E. B. Monteath 1
Dr. Kurt Rothe,
Chief, Turbomachinery 1

TAPCO Division
TRW, Incorporated
23555 Euclid Avenue
Cleveland, Ohio 44117
Attn: P. T. Angell 1

Research Laboratories
United Aircraft Corporation
400 Main Street
East Hartford, Conn. 06108
Attn: Erle Martin 1

Worthington Corporation
Advance Product Division
Harrison, New Jersey
Attn: W. K. Jekat 1